INVESTIGATION OF THE HISTORY OF EXHUMATION AND FAULTING IN THE RUBY MOUNTAINS METAMORPHIC CORE COMPLEX, NEVADA

By

VIRGINIA NEWMAN

A THESIS PRESENTED TO THE GRADUATE SCHOOL
OF THE UNIVERSITY OF FLORIDA IN PARTIAL FULFILLMENT
OF THE REQUIREMENTS FOR THE DEGREE OF
MASTER OF SCIENCE

UNIVERSITY OF FLORIDA

2008

To my husband, Lou and my daughters, Hannah and Rachel

ACKNOWLEDGMENTS

First and foremost, I would like to express my gratitude to Dr. David Foster, my advisor, for his guidance and expertise during the process of this study. I also thank Dr. Keith Howard for sharing his knowledge of the geology of Ruby Mountains as well as his assistance in the field. I thank the many excellent professors I have had in the program, including Dr. Smith and Dr. Randazzo, my field camp instructors. I appreciate Dr. Neuhoff and Dr. Meert, my committee members, for their patience and assistance. I am extremely thankful to Mike Hartley, who assisted with many aspects of the lab work, and to Jennifer Gifford, who contributed GIS distances to this project. I would especially like to thank my husband for his financial support and patience.

Field work for this project was funded by the USGS. USGS also funded a portion of the fission-track analysis.

TABLE OF CONTENTS

LIST OF TABLES

LIST OF FIGURES

Abstract of Thesis Presented to the Graduate School
of the University of Florida in Partial Fulfillment of the
Requirements for the Degree of Master of Science

INVESTIGATION OF THE HISTORY OF EXHUMATION AND FAULTING IN THE RUBY MOUNTAINS METAMORPHIC CORE COMPLEX, NEVADA

By

Virginia Newman

May 2008

Chair: David Foster
Major: Geology

New $^{40}Ar/^{39}Ar$ and apatite fission-track data from the Ruby Mountains metamorphic core complex, in NE Nevada, helps to constrain the exhumation and cooling history of the area. Apatite fission-track data yielded a low-temperature history of exhumation along the west-rooted detachment fault flanking the range. Apatite results indicated rapid cooling in the Miocene and also provided apparent ages of samples along a transect perpendicular to the fault. The change in apatite apparent ages with respect to elevation suggest that rapid cooling started at approximately 15 Ma. Sampling perpendicular to the direction of fault slip allowed for the calculation of an average rate of slip along the fault of 9.1 ± 3.1 km/my, assuming that the apparent ages reflect exhumation due to detachment slip. Biotite $^{40}Ar/^{39}Ar$ total fusion ages were determined from the same samples, and were also used to calculate a rate of slip along the fault. A rate of 1.6 ± 2.2 km/my was calculated from the biotite $^{40}Ar/^{39}Ar$ data. Due to the suspicion that some of the biotite samples were in the biotite argon partial retention zone, which would cause these samples to appear older than samples closer to the fault due to the fact that the original argon was not lost, a rate of 2.4 ± 0.6 km/my was recalculated using the younger biotite ages. The biotite $^{40}Ar/^{39}Ar$ data suggest that exhumation was accomplished mainly by tectonic denudation along a

detachment fault rather than erosion. The vertical variation of fission-track ages alternately suggest that these data record erosional exhumation due to erosion following the uplift of the footwall block relative to the adjacent valley floors. New data from this study as well as previous data indicate that rapid tectonic exhumation started at ca. 24 Ma and continued until ca. 14 Ma.

CHAPTER 1
INTRODUCTION

Metamorphic core complexes are the tectonically exhumed and highly extended footwalls of low-angle detachment normal faults (Crittendon et al., 1978). While it is known that these features form during continental extension, the processes that lead to core complex formation, as opposed to more distributed extension, are not yet resolved (Buck et al., 1988). In the Basin and Range province of the western United States, Tertiary metamorphic core complexes were exhumed during regional extension possibly caused by hot spot movement (Best et al., 1991), the growth of a subduction slab-gap (Sonder and Jones, 1999), a relaxation of boundary forces (Sonder and Jones, 1999), or the orogenic collapse of overly thickened crust (Coney and Harms, 1984).

The timing of the onset of extension in many of the metamorphic core complexes in the central and northern Basin and Range, south of the Snake River Plain, is poorly constrained. Some place the onset of extension in the northern Basin and Range between 55 to 45 Ma (Sonder and Jones, 1999; and McGrew et al., 1994). Others contend that most extension did not start until the Miocene (Stockli et al., 2001; and Dokka et al., 1986). The confusion within the timing of these events arises from the multiple episodes of extension that are overprinted in the area (Dallmeyer et al., 1986; and Mueller et al., 1999). The issue is complicated further by the possibility of distinctly different processes initiating and perpetuating extension at different times. Some researchers believe there was an earlier period of extensional thinning of the ductile middle crust followed by a later period of extension of the entire crust (Wells et al., 2000).

The Ruby Mountains, which are the focus of this study, are part of the southernmost extent of the northern Basin and Range Province, located in northeast Nevada (Fig. 1). Previous research in the Ruby Mountains Metamorphic Core Complex documented gradual cooling of

rocks that were at the upper middle crust in Late Cretaceous time, from 63 to 49 Ma (Mueller et al., 1999). Data from the same study shows that deeper structural levels cooled rapidly between 36 to 29 Ma, with all rocks exposed in the core complex footwall being cooled at or below the 100° C isotherm by ca. 23 Ma (Mueller et al., 1999). There is disagreement, however, about the actual timing of rapid cooling. Dallmeyer et al. (1986) place the period of rapid cooling between 20 to 30 Ma, with all rocks cooled below 100ºC by ca. 20 Ma. Reese (1983) discusses two distinct episodes of extension occurring in the Ruby Mountains footwall. The first occurred between ca. 37 to 30 Ma, followed by a second between ca. 25 to 9 Ma after a tectonic hiatus. Hodges et al. (1992) suggests that unroofing began during and immediately following Late Cretaceous thrust burial, but most thermochronological data indicate major exhumation and cooling in Oligocene and Miocene epochs (Mueller et al., 1999; Hurlow et al., 1991; Reese, 1983). Biotite K-Ar ages from the eastern Ruby Mountains record cooling below approximately 300°C between ca. 37.6 and 30.1 Ma, which could indicate Oligocene extension or be related to an exhumed partial retention zone. The kinematics of detachment normal faults and timing of cooling indicate that exhumation was derived by tectonic extension and that the footwall rocks in the Ruby Mountains form a metamorphic core complex (Howard, 1980).

Rocks exposed in the Ruby Mountains were exhumed from depths of as much as 35 km following burial by thrusting in the Late Cretaceous (McGrew et al., 2000). The metamorphic core complex is flanked by a west-rooted, low-angle, mylonitic detachment fault that is overlain by a more complex arrangement of normal and listric faults. The complex arrangement of high-angle faults overlying low-angle detachment formed as the nonrigid footwall was exhumed from beneath the hanging wall along a low angle detachment fault (Howard, 1980).

The current body of knowledge existing on the timing and rates of extension in the Ruby Mountains was obtained through previous thermochronologic studies, using the K-Ar and fission track methods (Dallmeyer et al., 1986; Dokka et al., 1986; Reese, 1983; McGrew et al., 1994). The use of several thermochronologic systems together to study core complex footwalls allows the reconstruction of a thermal history over a larger temperature range than one system alone (Foster and John, 1999; Stockli, 2005). Each unique thermochronologic system can provide information about the timing of the cooling of a rock body through the specific closing temperature of the minerals in question and thereby the exhumation of footwall rocks from different paleodepths. Additional information about the meaning of rocks cooling histories can be obtained by integrating geologic and structural information obtained in the field.

Published K-Ar and $^{40}Ar/^{39}Ar$ apparent ages and apatite fission track apparent ages in the Ruby Mountains core complex footwall young westward in the direction of extensional unroofing for each mineral analyzed. Biotite $^{40}Ar/^{39}Ar$ apparent ages generally range from about 45 Ma to near ca. 20 Ma (Dallmeyer et al., 1986; Kistler et al., 1981; McGrew et al.,1994). If the previous biotite K-Ar apparent ages represent rapid cooling through the argon retention isotherm of about 300˚C, then the westward-younging pattern can be used to determine the rate of unroofing and quenching of the core complex. The approximate rate of fault slip can be obtained by inverting the rate of lateral change in cooling rate with distance (Foster et. al., 1993). Inversion based on the previous data indicates a rate of slip on the detachment of 1 to 2 km/m.y. A calculated rate of 1 to 2 km/m.y. indicates an onset to extension of around 30 to 25 Ma rather than 50 to 45 Ma. This apparent slip rate is several times slower than the rates of detachment slip in tectonically analogous areas, such as the Snake Range metamorphic core complex (Lee et al., 1991) and the Colorado extensional corridor (Foster et al., 1993; Foster and John, 1999),

which have calculated rates of 7 to 14 km/m.y. The calculated rate of extension in the Ruby Mountains is also an order of magnitude slower than the rates estimated from shear-strain fabrics in the mylonitic shear zone that roofs the core complex, which suggests extension occurred at a rate of 22 km/my (Hacker et al., 1990). The calculated rate also does not account for the peak time of rapid quenching in the Ruby Mountains and regionally, which apparently occurred in the middle Miocene, approximately 24 Ma (Dokka et al., 1986; Stockli et al., 2001). Furthermore, the extension rate would have had to be many times faster to exhume the full 35 km if all the extension occurred in one event. The resolution of this contradiction is a principle reason for the study. The calculated rate of extension may also support or refute one or more of the previously discussed hypotheses relating to possible causes of extension in the area.

I present new apatite fission track and $^{40}Ar/^{39}Ar$ thermochronometry that constrain the timing of onset of extension and the rate of slip along the low angle detachment fault flanking the Ruby Mountains metamorphic core complex. The data and conclusions generated by this study compliment recent and ongoing thermochronologic studies in the Basin and Range (McGrew et al., 2000; Colgin et al., 2006). These combined data have important implications for the cause of widespread extension in the Basin and Range during Neogene times, because they reveal the spatial distribution of the timing of extension and exhumation of a spectrum of crustal levels.

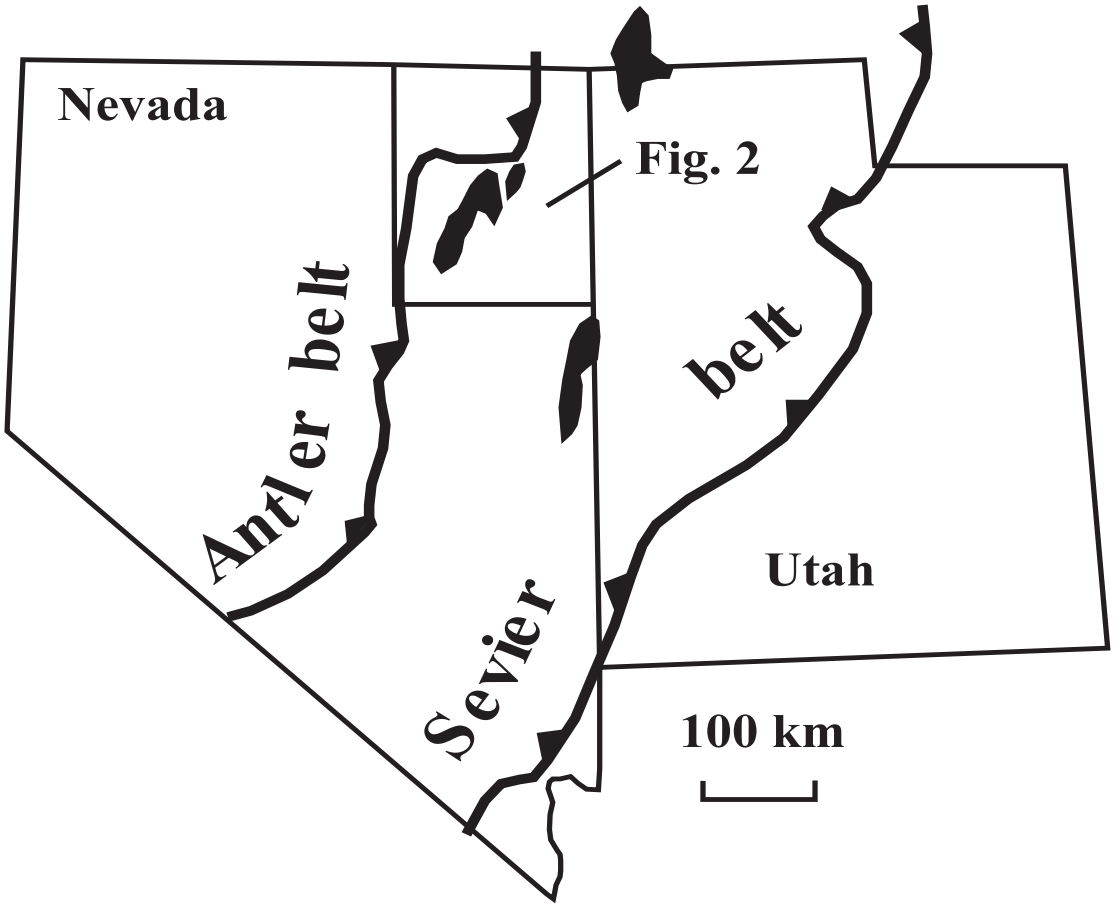

Figure 1-1. Location map of the Ruby Mountains metamorphic core complex, located in northeast Nevada between the Antler orogenic belt and the Sevier orogenic belt.

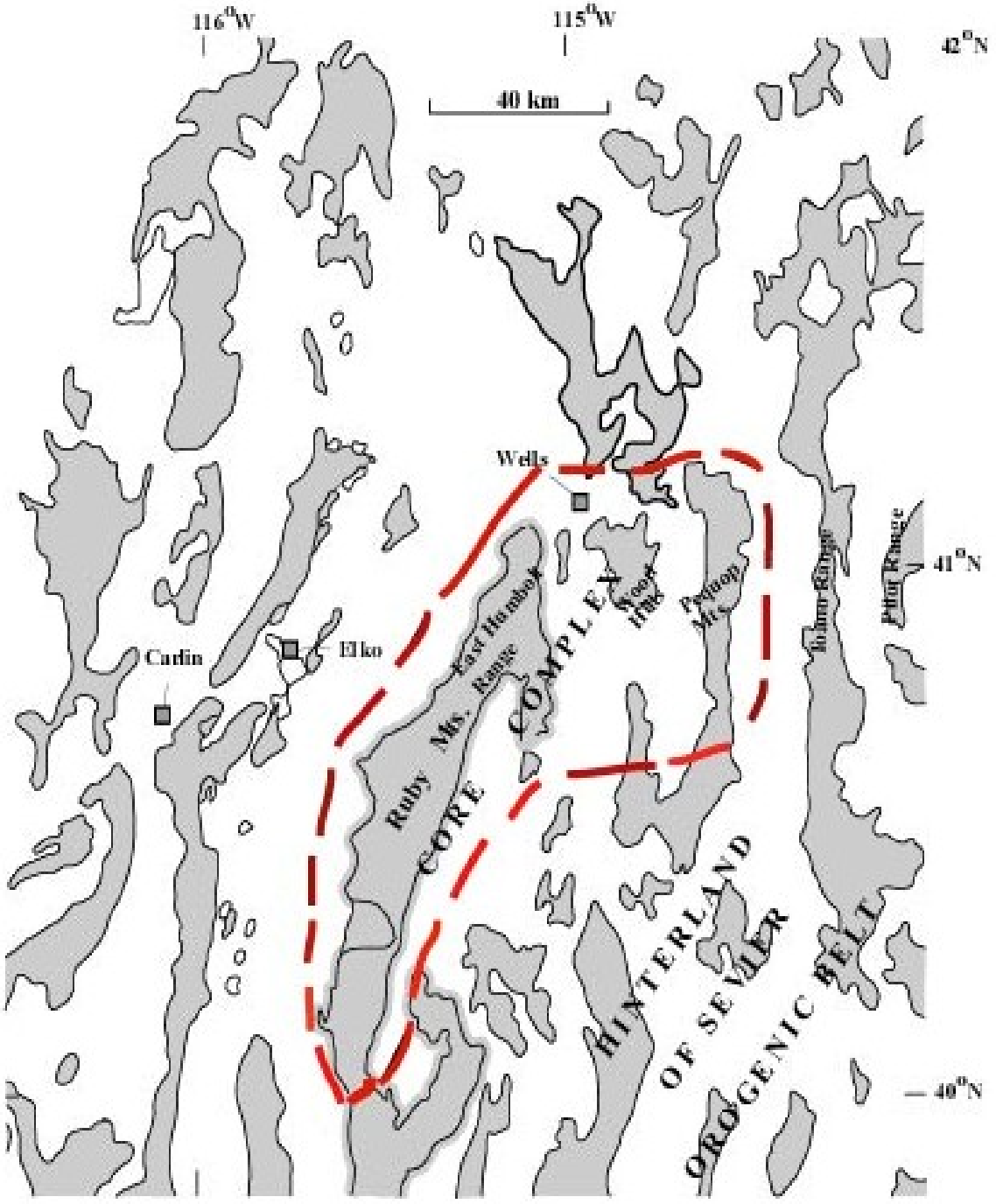

Figure 1-2. Map of the Ruby Mountains metamorphic core complex region, including the Ruby Mountains- East Humboldt Range, Clover Hill, Wood Hills, and a portion of the Pequop Mountains, outlined in the dashed red line. Gray areas represent ranges in the area.

CHAPTER 2
GEOLOGIC SETTING

Regional geologic background

The Cretaceous Sevier Orogeny in NE Nevada was characterized by large scale thrusting of miogeoclinal sediments, along with extensive ductile deformation, granitoid intrusion, and metamorphism. By the end of the Sevier Orogeny the crust in central Nevada could have been as thick as 60 to 70 km (Burchfiel et al., 1992). In Latest Cretaceous time the convergence rate of the Faralon and North American plates increased and the dip of the subducting slab decreased (Armstrong and Ward, 1991). This resulted in the migration of the magmatic arc to the east and further crustal shortening. Rocks now exposed in the footwall of the Ruby Mountains core complex represent the once deeply buried core of the Servier-Laramide Orogen. These rocks underwent metamorphism, thrusting, nappe folding, and the intrusion of granitic rocks during this event (Howard, 1980).

Laramide deformation continued into the early Cenozoic. At this time, the entire length of the western edge of North America was a convergent plate boundary, with the North American plate overriding the Faralon plate (Sonder and Jones, 1999). The dip of the subducting slab steepened in the Nevadan part of the orogen about 40 Ma, shifting magmatism westward, and shrinking the magmatic gap that had been caused by shallow subduction. A period of intense magmatic activity, known as the ignimbrite flare-up, ensued in the Great Basin around 40 Ma (Armstrong and Ward, 1991). Magmatism gradually migrated west, as the dynamics of the plate boundary changed (Sonder and Jones, 1999). The previously thickened lithosphere was thermally weakened due to magmatism and/or asthenospheric upwelling (Armstrong and Ward, 1991). The convergent boundary was gradually replaced by right-lateral transform motion as the Mendocino triple junction moved to the north. The switch from a convergent boundary to a

transform boundary resulted in the formation of the San Andreas fault system, the opening of the Gulf of California, and a change in boundary forces acting on the plates. Large scale extension in the northern Basin and Range (NBR) could have begun as early as the middle-late Eocene (Sonder and Jones, 1999). Total extension across the Nevada segment of the Basin and Range province has been estimated to be 120 to 150 km (Gans 1987; Wernicke 1992).

Geologic History of the Ruby Mountains Metamorphic Core Complex

The Ruby Mountains Metamorphic Core Complex is located east of the Paleozoic Antler orogenic belt, and west of the Mesozoic Sevier belt (Howard, 1980) (Fig 1). Rocks exposed in the East Humboldt Range, Clover Hill and Wood Hills are also part of the metamorphic core complex footwall (Fig.2). The deepest structural levels exposed in the region lie in the East Humboldt range and the Clover Hill area. Structurally shallower-level strata are exposed in Wood Hills and the Pequop Mountains, to the east of the Ruby Mountains. The northernmost exposure of rocks related to the core complex is located in the southern Windermere Hills (Mueller et al, 1993).

Geologic elements in this area can be divided into four separate subsets. The deepest structural levels are composed of metamorphic core complex rocks, including possible Precambrian basement rocks, Late Proterozoic to Mid-Paleozoic metasedimentary rocks, and Mesozoic and Tertiary igneous rocks. This suite of rocks comprises the migmatitic igneous and metamorphic infrastructure of the complex. An approximately 1 km thick mylonitic shear zone overlays and deforms the upper portion of the metamorphic and igneous infrastructure. The mylonitic shear zone is structurally beneath a highly extended cover sequence of unmetamorphosed to low-grade metamorphic Paleozoic through Tertiary strata (Mueller et al, 1993; MacCready, 1997). In the Northern Ruby Mountains and East Humboldt Range a low-angle normal fault system separates the core complex from low-grade metamorphic rocks. In

more southerly portions of the complex these cover rocks are transitional into the metamorphic rocks.

The focus of this study is on a cross-section through the center part of the range at Lamoille Canyon, which is an excellent location to study the low-angle detachment system because all of the structural elements are exposed. The cross-section is along a road to Lamoille Canyon, which was carved by the Lamoille Canyon glacier. This glacier deposited moraines approximately 12 miles long (Sharp, 1938), which are cut by fault scarps, indicating that brittle faulting continued into the Holocene.

The mylonitic zone is exposed along the west range front. The mylonite transition zone is approximately 1 km thick along the western flank of the mountain range. Features such as asymmetric mica porphyroclasts and asymmetric parasitic folds within the micaceous mylonite indicate a west-northwest sense of shear. Stratigraphic sequences in the mylonite zone have been tectonically thinned as much as one-fifteenth to one-twentieth of the original thickness. Metamorphic barometry studies indicate that Neoproterozoic strata were buried as much as 35 km (Hodges et. al, 1992). Deformation in the mylonite zone occurred at amphibolites and greenschist facies conditions (Howard, 1980). The blastomylonitic fabric found in the transition zone most likely resulted from extreme tectonic flattening and stretching. Rocks at the base of the mylonite zone grade into the higher-grade, coarser-grained, nonmylonitic rocks of the metamorphic infrastructure.

At deeper structural levels beneath the mylonite zone, granitic dikes, sills and irregular bodies form more than half the exposed rocks. The granitic rocks are predominantly two-mica granite, but granodiorite gneiss, biotite granite, and local bodies of metagabbro are also present. Two-mica granites in the area are small discontinuous bodies so they generally are not mapped

separately from the metasediments that they intrude (MacCready et al., 1997). The exception is the leucogranite orthogneiss of Thorpe Creek, which occurs as a sheet like body in the core of the Lamoille Canyon Nappe. The granite in the area is predominantly Jurassic or Cretaceous in age, and appears to be sourced from metasedimentary rocks at an intermediate depth, though there is some Tertiary plutonic material as well. The percentage of granitic material increases in relation to the percentage metamorphic materials toward the deeper structural levels of the complex (Howard, 1980).

Metamorphic rocks in the footwall of the core complex include high-grade marble and quartzite. The marbles and quartzites can be roughly correlated to the unmetamorphosed Paleozoic shelf sediments in the hanging wall (Howard, 1971). The oldest stratigraphic unit is the lower Cambrian Prospect Mountain Quartzite. The unit directly above the Prospect Mountain Quartzite is a calc-silicate marble correlated with Cambrian limestones and shales and the Ordovician Pogonip group. The Eureka Quartzite overlays the marble. Immediately above the Eureka Quartzite is a massive, white, nearly pure dolomite unit. The uppermost unit is a color-banded marble that correlates to the Guilmette Limestone.

Several large recumbent folds exist within the footwall of the core complex. In Lamoille Canyon, the Lamoille nappe folds the premetamorphic Ogilvie Thrust, Prospect Mountain Quartzite, and Verdi Peak Marble into an eastward overturned recumbent anticline that plunges shallowly north (Howard, 1971). The recumbent folds may have been forged by diapers as the migmatite front moved toward more shallow structural levels (Howard, 1980), or by progressive shortening in the middle crust (Camilleri et al.1996; McCready et al., 1997).

Tertiary strata in valleys to the west of the Ruby Mountains include conglomerates with limestone clasts that were presumably derived from limestone cover that was structurally above

the core complex (MacCready et al., 1997). Younger Tertiary strata contain metamorphic and granitic clasts derived from the Ruby Mountains.

CHAPTER 3
METHODS

Twelve samples of amphibolite and granite were collected on a slip-orthogonal transect representing progressively shallow to deep structural levels in the footwall of the low-angle detachment fault flanking the Ruby Mountains (Table 1; Fig.4). Granitic samples were separated for apatite, mica and potassium feldspar using standard density and magnetic methods (Appendix A) during the fall of 2002 and spring of 2003. Amphibolite samples were processed for mica, apatite, and amphibole.

Biotite samples were irradiated at Oregon State University and analyzed by the $^{40}Ar/^{39}Ar$ method in the noble gas laboratory at the Department of Geological Sciences at the University of Florida in the spring and summer of 2004. Biotite samples were fused in a water-cooled double-vacuum furnace to extract argon gas from the samples. The biotite samples were fused due to the tendency of biotite to become unstable during the step heating process and the likelihood the fusion age would be the same as the plateau age (McDougall and Harrison, 1999).

Argon gas extracted from the samples during furnace heating was transferred through vacuum lines and exposed to getters for ten minutes to remove reactive gases. The purified argon gas was analyzed in a Mass Analyzer Products Model 215-50 mass spectrometer using a Balzers electron multiplier to measure ion beams of ^{36}Ar, ^{37}Ar, ^{38}Ar, ^{39}Ar, and ^{40}Ar. Blanks were performed at the beginning of each day, and periodically between samples. Data were reduced using the program ArArCALC version 2.2 by Koppers (2002). ArArCALC utilizes Excel© by Microsoft to calculate apparent ages, plot age plateaus, and isochrons. The ArArCALC program was also used to calculate J-values from total fusion ages of the GA1550 biotite flux monitors. These calculated J-values were then utilized in the calculation of $^{40}Ar/^{39}Ar$ total fusion age calculations.

Fission-track analysis of apatite samples was performed by Ray Donelick at Apatite to Zircon, Inc. during the spring and summer of 2003. Suitable grains were polished to an internal surface that intersected fission-tracks from above and below the polished plane equally. The fission-tracks were etched in 5.5 M HNO_3 for 20 seconds at 21°C. The resultant etched tracks were then viewed using an unpolarized light microscope at 1562.5x or 2000x magnification from grains free of large surface imperfections and possessing a minimum of inclusions and crystal defects. The number of spontaneous fission-tracks counted over a selected area of the grain divided by the area itself yields the spontaneous fission-track density. The external detector method (EDM) was utilized to determine the relative uranium concentrations in the grains selected for analysis. The external detector was a low-uranium, fission-track free muscovite mica. The mica was placed adjacent to the apatite grain mount and both irradiated with thermal neutrons in a nuclear reactor (Donelick, 2005). The induced fission-tracks on the mica were then etched in 49% HF for 15 minutes at 23°C. Apatite age and length data were forward modeled using the Monte Trax program by Gallagher (1995), to estimate the thermal history of the samples. MonteTrax was used in the genetic algorithm mode with 100 simulations of 250 runs were used to calculate the best fit cooling lines included in Appendix C.

Table 3-1. Rock samples from the Ruby Mountains, Nevada

Sample number	Rock type*	El. (m)	UTM_N	UTM_E
H93 RBY-4	Tm, biotite granodiorite	3039	4501690	637380
H93 RBY-5	Tum, amphibolite	3017	4501735	637100
H93 RBY-8	Ocm Bio. Amphibolite	2561	4498710	638150
H97 RUBY-41	Kp, leucogranite	1895	4496400	644800
H97 RUBY-42	Kp, leucogranite	2088	4497130	642225
H97 LC-51	Tg bio-gar aplite, folded	2981	4494900	638730
H97 LC-52	Kp,pegmatitic granite gneiss	2434	4499050	637900
H97 RUBY-53	CZp, micaceous quartzite	2310	4501000	635320
H97 RUBY-54	Tm, biotite granite	2010	4503740	629685
H97 RUBY-55	mylonitic granite gniess	1905	4505645	628630

Samples H93RBY-4, H97 LC-51, and H97 RUBY-54 are probably ca.29 intrusions. All samples were collected on a cross-strike traverse approximately 20km long. Abbreviations of rock units as indicated on Figure 3-1.

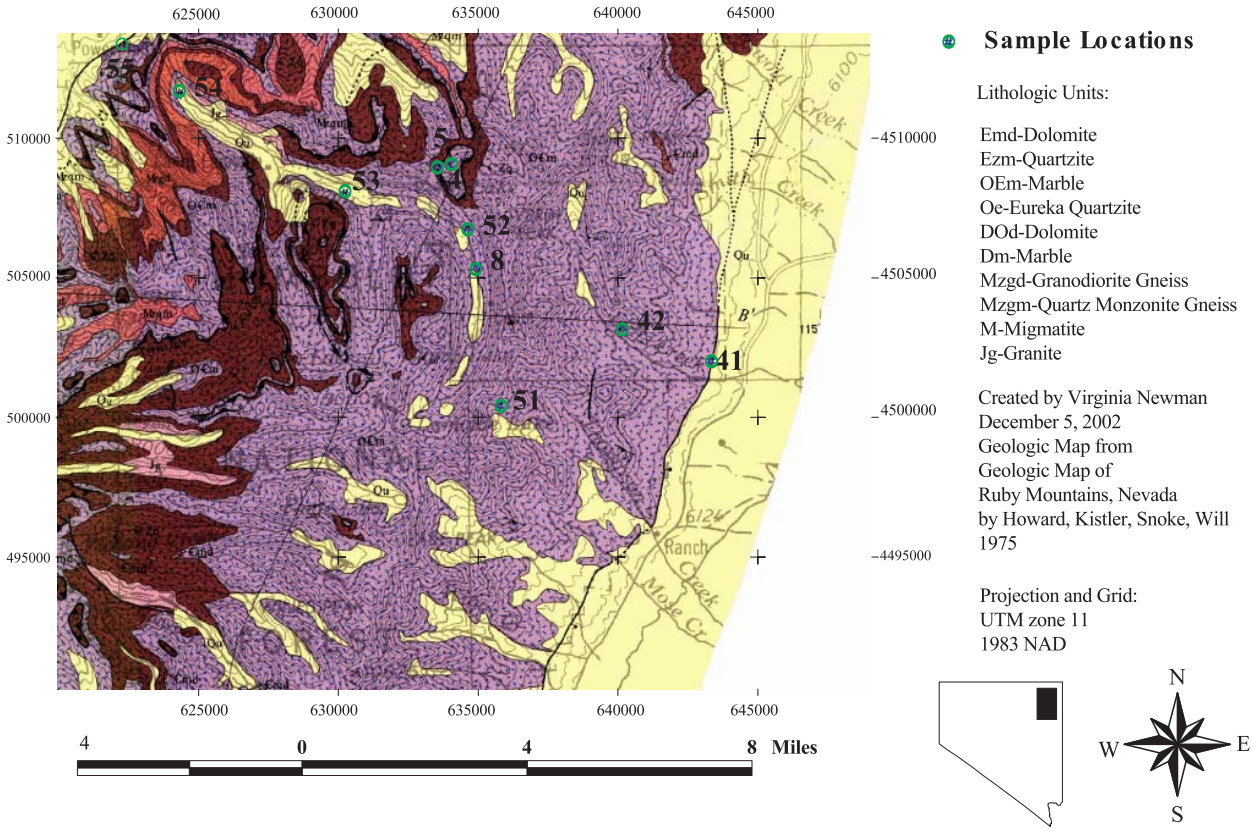

Figure 3-1. Lamoille Valley thermochronology sample locations

CHAPTER 4
APATITE FISSION-TRACK RESULTS

Apatite fission track data are useful for reconstructing low-temperature thermal histories of rock masses due to the low blocking temperature (Gleadow and Brown, 1999; Gallagher et al., 1998; Stockli, 2005). The closing temperature for fission-tracks in apatite is approximately 110ºC ± 10ºC for geologically rapid cooling rates (Gleadow and Duddy, 1981). In reality, fission-tracks anneal progressively through a temperature interval called the partial annealing zone (PAZ). The temperature range is from approximately 60°C to 110°C for common compositions of apatite, with annealing occurring more rapidly at the upper end of this range (Gleadow, and Brown, 1999; Stockli, 2005). Fission-track dates may be combined with estimates of the geothermal gradient to obtain information about the rate of exhumation and erosion. In addition to obtaining the date at which a grain cooled through the closing temperature, much information about the cooling history of a sample can be obtained by analyzing the distribution of fission-track lengths.

Previous studies in the Ruby Mountains yield fairly consistent apatite fission-track dates. A study by Dokka et al., (1986) showed a range in fission-track ages for titanite, zircon, and apatite from 24 ± 2 to 18 ± 2 Ma from samples taken in the northern Ruby Mountains, north of Lamoille Valley. These data suggested that rapid cooling started between ca. 25 and 23 Ma, and that rocks had cooled from above approximately 300°C to below 70°C between approximately 24 to 18 Ma. Previous apatite fission-track studies performed by the population method done in Lamoille Valley yielded apatite ages of 12 ± 5, 15 ± 2, 18 ± 2 Ma (Reese, 1983). The ages increase from west to east along a transect through Lamoille Valley. Reese (1983) estimates apparent rate of exhumation of 87 m/my or .087 km/my from these results. Unfortunately, the

population method is known to bias age estimates and no track length measurements were made in this study, so the rate of cooling could not be assessed.

Samples collected for this study were obtained along a west to east transect through Lamoille Valley, perpendicular to the detachment fault along the western flank of the range. Samples were collected in this way to show the change in age as a function of distance from the fault (Fig. 3-1). Apatite data obtained from 9 of 12 samples collected from the Lamoille Canyon area is summarized in Appendix B. The samples yielded high quality apatite with abundant tracks and gave reliable data. Apatite fission track ages ranged from 21.1 ± 1.5 Ma to 14.4 ± 1.9 Ma. All samples yielded unimodal track length distributions with mean lengths between about 14.1 to 14.9 microns. These long track lengths indicate rapid cooling rates and that the fission-track ages reflect cooling through the partial annealing zone. The apparent ages of each sample were plotted in ISOPLOT (Ludwig, 2004), in terms of elevation and in terms of distance from the detachment to shed light on the possible causes and rates of exhumation (Figures4-1 and 4-2).

The graph of apparent apatite ages vs. sample elevations indicates rapid cooling at approximately 15 Ma (Figure4-1), with the exception of samples H97 RUBY-41 and H97 RUBY-54. This relationship suggests a possible second episode of cooling at ca. 15 Ma. It should be noted that sample H93 RBY-8 was severely weathered, showing signs of extensive oxidation. Samples H93 RBY-4, H97 LC-51, and H97 RUBY-54 were collected from Tertiary plutons, but this should not affect the results because the intrusion ages of the plutons are much older than the timing of cooling and exhumation. The age of rapid cooling generally increases as the distance from the fault increases, but the relationship is partially obscured by the large errors

(Figure4-2). This suggests that exhumation progressed from east to west due to movement along the detachment.

Model cooling histories and track length distributions were calculated using Montetrax (Appendix C). The mean fission-track lengths obtained from each sample ranged from 14.06 μm to 14.86 μm. The long mean track lengths and unimodal track distributions indicate a straightforward cooling history without the influence of any thermal anomalies (Gleadow et al., 1986). The T-t models reveal rapid cooling through the PAZ (110°-60°C) centered at the apparent age of the samples. Calculated model track length distributions are consistent with the observed data.

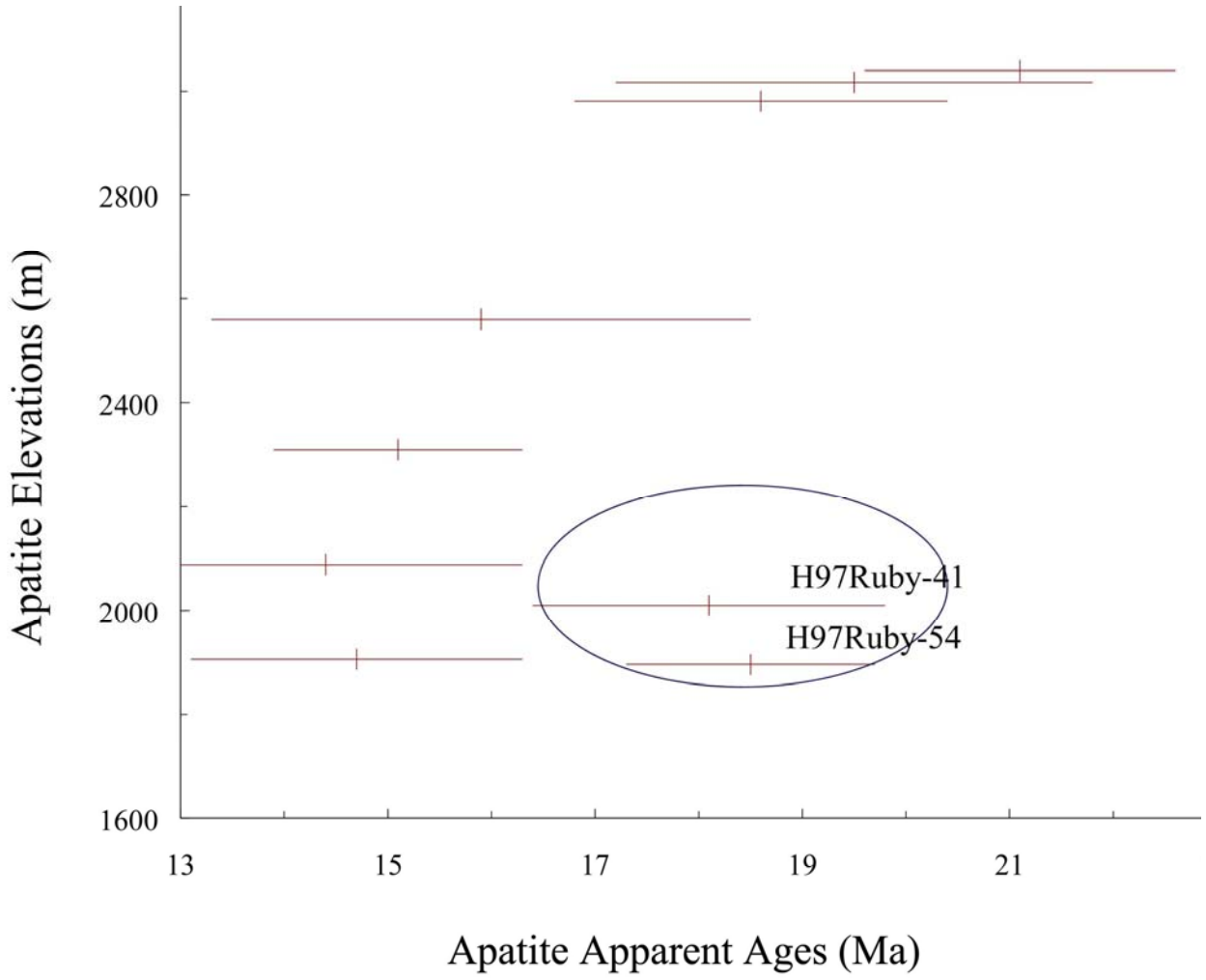

Figure 4-1. Apatite apparent ages vs. sample elevation. This graph is a x-y plot constructed in Isoplot. H97 RUBY-41 and H97 RUBY-54 are contained in the blue ellipse as exceptions to the apparent cooling trend at ca. 15Ma. Apparent age errors are listed in Appendix B, elevation errors are 20m. Error crosses are 2σ.

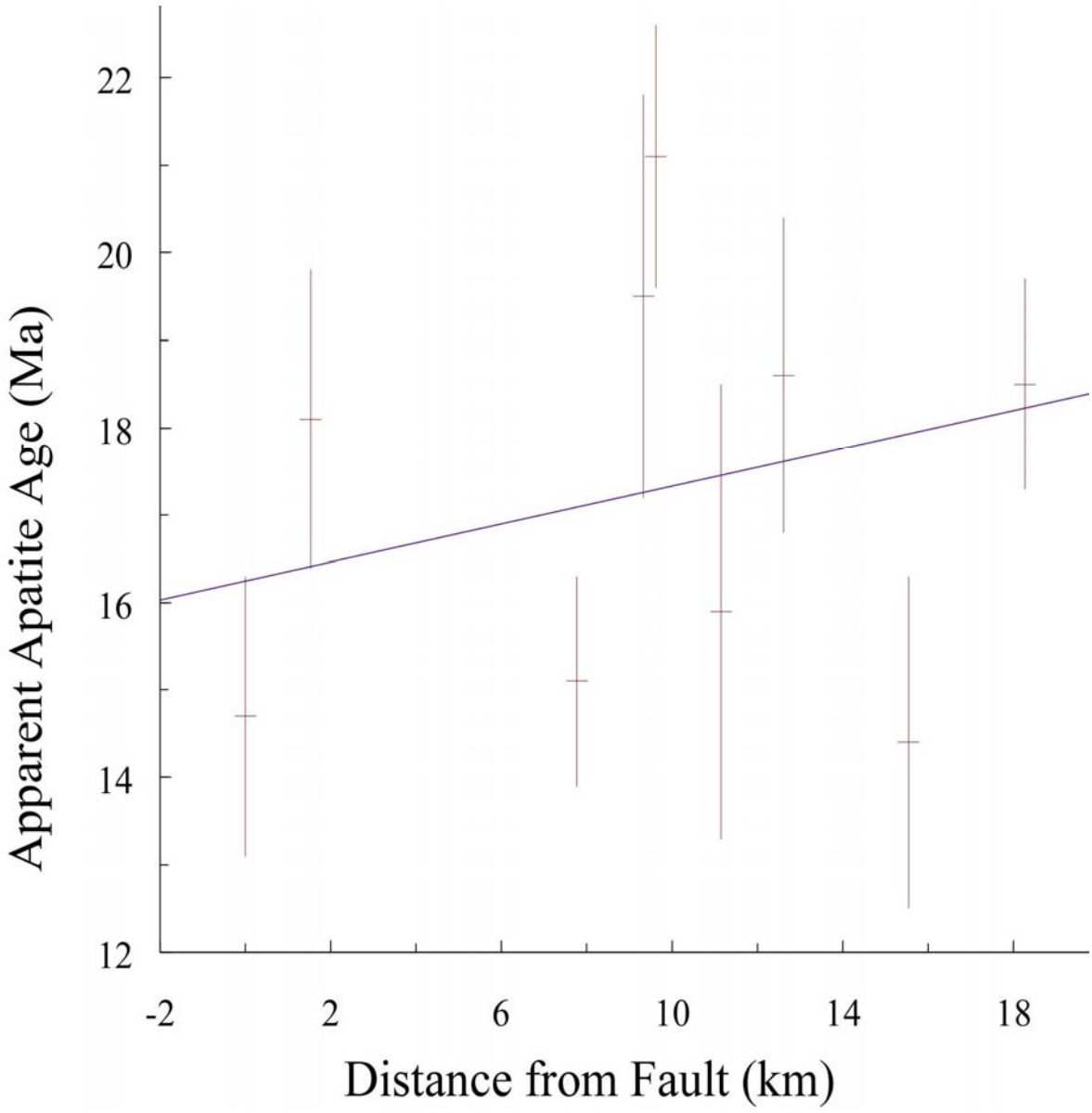

Figure 4-2. Apatite apparent ages vs. distance from fault. This figure was generated in Isoplot. Data points were plotted in an x-y graph and the regression line was drawn using x-y weighted averages. Apparent age errors are taken from Appendix B, distance errors are .25km. The slope of the regression line is 0.11 ± 0.32. Mean Squared Weighted Deviates (MSWD) for the regression is 9.3. Error crosses are 2σ.

CHAPTER 5
BIOTITE $^{40}AR/^{39}AR$ RESULTS

Previous studies using the $^{40}Ar/^{39}Ar$ method on biotite in the Ruby Mountains core complex produced predominately Oligocene and earliest Miocene ages. These results are interpreted to indicate cooling below the argon closure in biotite or about 300°C (McDougall and Harrison, 1999). Studies by McGrew et al. (1994) yielded $^{40}Ar/^{39}Ar$ mica ages between 21.7 ± 0.2 Ma and 22.9 ± 0.3 Ma. The same study found that rapid cooling from approximately 300°C to below 100°C occurred by 20 Ma. Dallmeyer et al. (1986) obtained argon ages from biotite samples both in the mylonite zone and above it. Above the mylonite zone ages ranged from approximately 32 to 33 Ma. Within the mylonite zone ages were younger, ranging from approximately 22 to 24 Ma. Specifically in Lamoille Canyon, a biotite from non-mylonitic rock produced an age of 25.3 ± .7 Ma. A biotite from within the mylonite, in Lamoille Valley yielded an age of 20.8 ± .5 Ma. The authors postulate that rapid cooling began by approximately 45 Ma and that the rocks had cooled to below 300°C by 20 Ma. Biotite data published Kistler et al. (1981) and utilized by Reese (1983) from Lamoille Valley yielded ages from ca. 19.6 to 33 Ma, going generally from youngest to oldest in a west to east fashion.

Samples for this study were collected along a slip orthogonal transect through Lamoille Valley to avoid along-strike variations in cooling or exhumation history (Fig.3-1). This provides for the determination of the change in age of samples as a function of distance from the exposed trace of the detachment fault. Biotite was separated using standard density and magnetic methods from the same samples used for apatite fission-track analysis (Appendix A).

$^{40}Ar/^{39}Ar$ total fusion ages for the eight samples range from ca. 31.0 to 20.7 Ma (Table 5-1). The total fusion ages are in general agreement with dates obtained from previous studies (Dallmeyer et al., 1986; McGrew et al., 1994,). The biotite ages were graphed in ISOPLOT

(Ludwig, 2004) against sample elevations and the distance of rocks sampled from the fault to aid in determine the rate and cause of rapid extension in the area (Figs. 5-1 and 5-2).

The graph of biotite ages vs. sample elevation shows no clear relationship between biotite apparent age and sample elevation (Fig. 5-1). The biotite apparent ages are older than the apatite fission-track ages from the respective samples, due to the higher closure temperature of biotite, approximately 300º C vs. 100º C. When biotite ages are graphed against distance from the fault a trend does emerge (Fig. 5-2). The cooling ages generally increase with distance from the fault, indicating that exhumation progressed from east to west along the detachment.

Table 5-1. Biotite 40Ar/39Ar total fusion ages

Sample number	Total fusion age (Ma)	error±2σ (Ma)
H93 RBY-4	23.06	1.04
H93 RBY-8	30.92	1.75
H97 RUBY-42	31.24	1.75
H97 LC-51	31.26	1.53
H97 LC-52	27.06	1.17
H97 RUBY-53	24.44	0.83
H97 RUBY-54	24.68	2.16
H97 RUBY-55	20.7	0.98

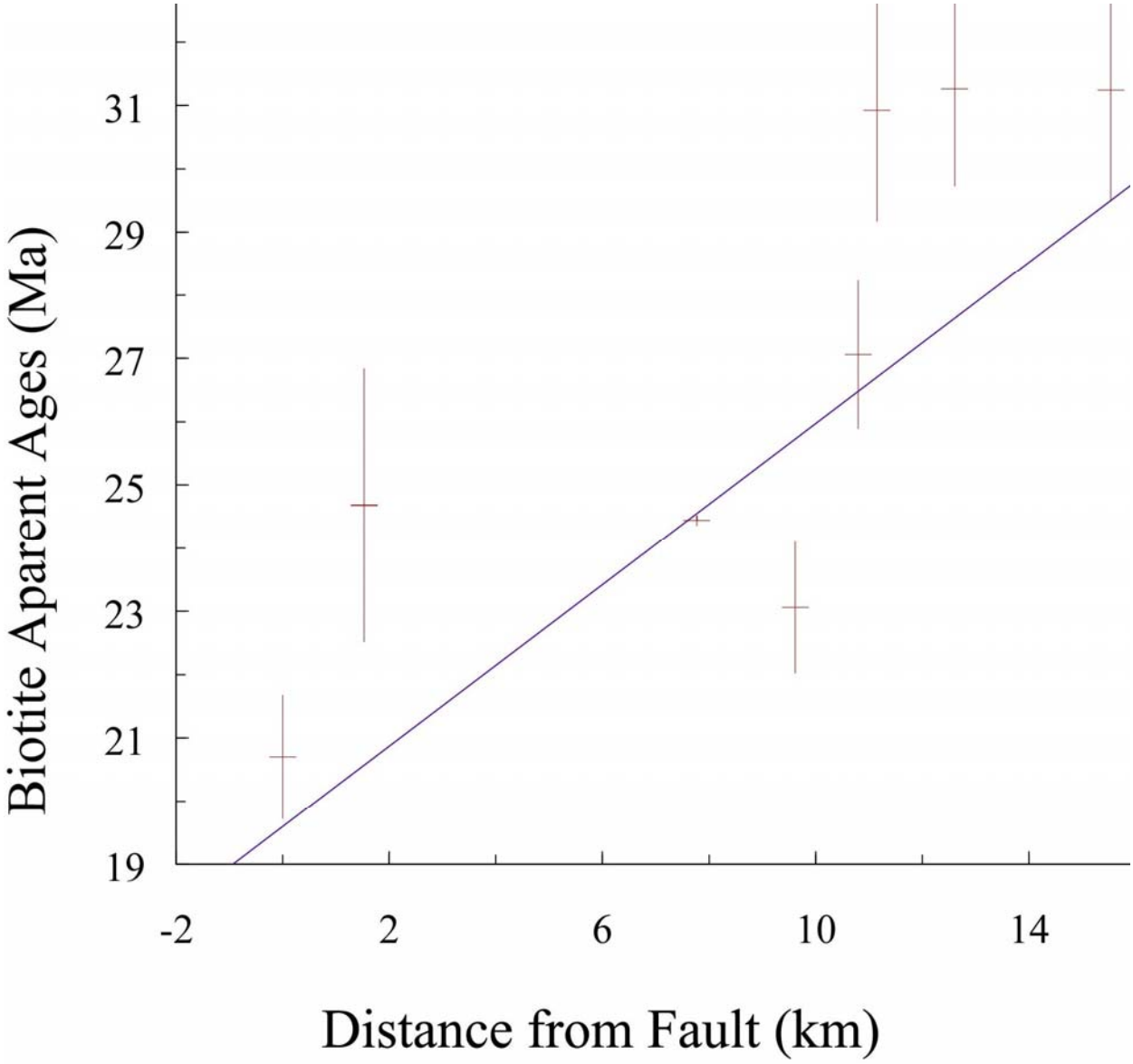

Figure 5-1. Biotite apparent ages vs. elevation. This graph was generated in Isoplot in a x-y plot. Age errors are from Table2, elevation errors are taken to be 20m. Error crosses are 2σ.

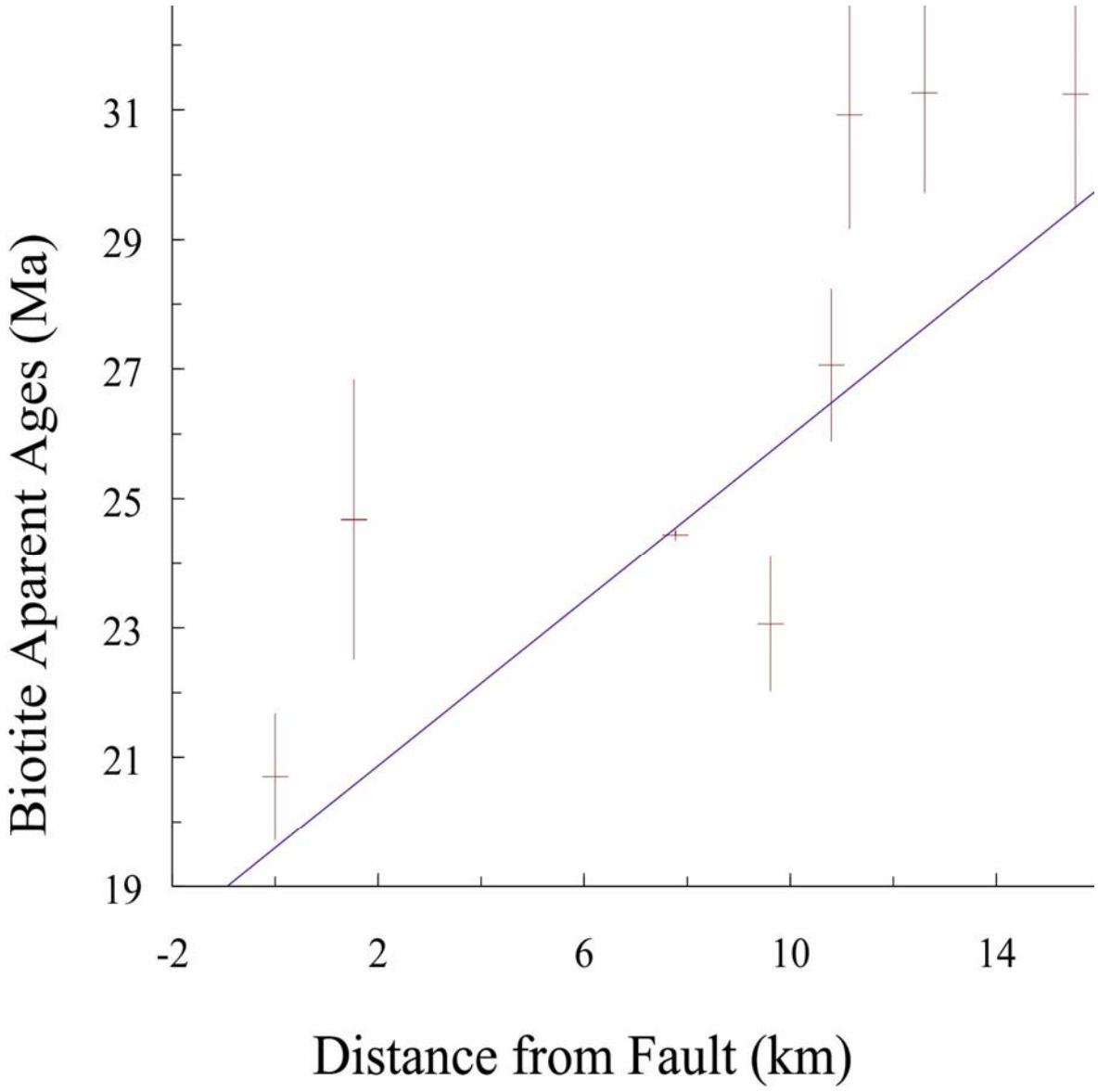

Figure 5-2. Biotite apparent ages vs. distance from fault. This figure was generated in Isoplot. Data points were plotted in an x-y graph and the regression line was drawn using x-y weighted averages. Apparent age errors are taken from Table 5-1, distance errors are .25km. The slope of the regression line is 0.64 ± 0.46. Mean Squared Weighted Deviates (MSWD) for the regression is 16. Error crosses are 2σ.

CHAPTER 6
DISCUSSION

The use of multiple isotopic systems and mineral phases for thermochronology research allows the reconstruction of thermal histories over a greater temperature range than one system alone (Foster and John, 1999; Stockli, 2005). Apatite fission-track data and thermal models show that exposed rocks along the Lamoille transect in the Ruby Mountains metamorphic core complex cooled below approximately 100°C between 21.1 ± 1.5 Ma in the east and 14.4 ± 1.9 Ma in the west (Appendices B and C). The early to middle Miocene cooling interval is in general agreement with other studies (Dokka et al., 1986; Reese, 1983), but is more precise and allows the progression of exhumation to be assessed.

Rapid cooling that progressed from east to west supports the hypothesis that the core complex was exhumed due to slip along an asymmetric detachment fault. Previously estimated rates of exhumation for this detachment system were generally 1 to 2 km/my (Reese, 1983; McGrew, 1994). The rate of extension calculated from these data was more rapid than suggested by previous studies that were based on fewer samples and more widely scattered sample locations. Apparent apatite ages vs. distance from the fault were regressed in ISOPLOT (Fig.4-2). The slope of the regression line generated by ISOPLOT is 0.11 ± 0.32. By inverting the slope and its error, the lateral rate of change, an approximate rate of 9.1 ± 3.1 km/my is given. This apparent slip rate is within a range of rates of detachment slip in tectonically analogous areas, such as the Snake Range metamorphic core complex (Lee et al., 1991) and the Colorado extensional corridor (Foster et al., 1993; Foster and John, 1999; Carter et al., 2006), where the rates are approximately 7 to 14 km/my. The differences between the previous estimate by Reese, 1983 and the data from this study are probably due to the bias introduced by the older population method. The slower rates may indicate different mechanisms for metamorphic core complex

development in the two areas, such as rolling hinge vs. low-angle detachment with two phases of cooling.

A possible second phase of brittle faulting and rapid exhumation is indicated by the relationship between apatite apparent ages and sample elevations (Fig. 4-1). H97Ruby-41 is the easternmost sample along the transect and has been down-dropped by range-front faults, explaining the older age of 18.1 ± 0.9 Ma at the lower elevation of 1895 m and its plotting outside of the rapid cooling trend. Sample H97Ruby-54 also plots outside this trend. With the exception of these two data, samples below 2600 m elevation give concordant ages. This suggests that rapid exhumation started at about 15 Ma due to erosion of the fault block.

Apatite fission-track and (U-Th)/He data published by Colgan et al., 2006 indicate that the southern Ruby Mountains, in the Harrison Pass region, was rapidly exhumed between 14-15 Ma. This data is an indication that the southern portion of the range was exhumed as an intact east-tilted block. The fault system in the Harrison pass area merges in the north with the mylonite zone that bounds the metamorphic core complex, indicating that rapid middle Miocene unroofing could have occurred in the northern part of the range as well (Colgan et al., 2006)

Biotite apparent ages vs. distance from the fault were also regressed in ISOPLOT (Fig. 5-2). The slope and error of the biotite regression line, 0.64 ± 0.46, was inverted and an apparent slip rate of approximately 1.6 ± 2.2 km/my was calculated. The west to east progression of biotite ages from younger to older also supports progressive exhumation due to slip along the detachment fault. The rate of extension calculated from these data was in agreement with previously calculated rates from biotite data, which were in a range from 0.1 to 1.5 km/my (Reese, 1983). The calculated rate based on the entire biotite $^{40}Ar/^{39}Ar$ data set is slower than expected when compared to the apatite fission track data.

Biotite and apatite data were graphed together to investigate possible reasons for the differences in the apparent slip rates calculated from each data set (Fig. 6-1). As expected, apatite ages were younger than biotite ages due to the lower closing temperature of apatite. However, it was expected that the biotite ages would be systematically older than the apatite ages. Instead, the difference between apatite and biotite ages increased as the distance from the fault increased. An explanation for the artificially high ages is that the older biotite ages, greater than about 24 Ma, at a distance of greater than 10 km from the exposed detachment were probably within the biotite argon partial retention interval prior to rapid extension starting at about 24 Ma (e.g. Foster and John, 1999). New biotite and muscovite $^{40}Ar/^{39}Ar$ produced by Jennifer Gifford at the University of Florida indicates two distinct episodes of extension and cooling (Gifford,J., 2008). If only the younger biotite ages are regressed due to the mixed cooling ages of the "older" samples, a rate of extension of 2.4 ± 0.6 km/my is given (Fig. 6-2). This rate is closer to the rate of slip calculated from the apatite data. These results are similar to the results from the Chemehuevi detachment in California (John and Foster, 1993), but are still slower than many detachment systems in the Basin and Range (Carter et al., 2004).

The significantly larger rate of slip along the detachment estimated from the apatite data could indicate that isostatic rebound played a role in unroofing the core complex. Variable rates of slip have been previously documented in the Harcuvar Mountains (Carter et al., 2004) and along the Chemehuevi and Sacramento detachment faults (Carter et al., 2006). The large rate may also indicate that some of the exhumation in this area was accomplished rapidly on brittle faults in the middle Miocene, rather than recording only the rate of slip along the low-angle detachment fault (Colgan et al., 2006).

The thermochronological data also reveal the time that rapid exhumation began and the duration of extension. All of the apatite fission-track ages have long track lengths with unimodal distributions, so they all reveal rapid cooling that must have started before ca. 20 Ma, the apparent age of the oldest sample. The biotite $^{40}Ar/^{39}Ar$ dates for samples greater than 10 km from the fault give apparent ages substantially older than the apatite fission-track ages, therefore, these record slower cooling. The biotite $^{40}Ar/^{39}Ar$ ages at approximately 10 km or less from the exposed fault are centered within error or a few m.y. older than the apatite fission-track ages. The oldest biotite age from the samples taken less than 10 km from the fault is ca. 24 Ma. A time of approximately 24 Ma is also at the transition in slope of the line between the ca. 30 Ma and the ca. 24 Ma biotites (Fig.6-3), which would record the 300º C isotherm prior to rapid extension (Foster and John, 1999). This also suggests that cooling initiated at ca. 24 Ma. This conclusion is consistent with previous studies (Dallmeyer et al., 1986; Dokka et al., 1986, McGrew, 1994), as well as new unpublished data obtained in the area (Gifford, J., 2008).

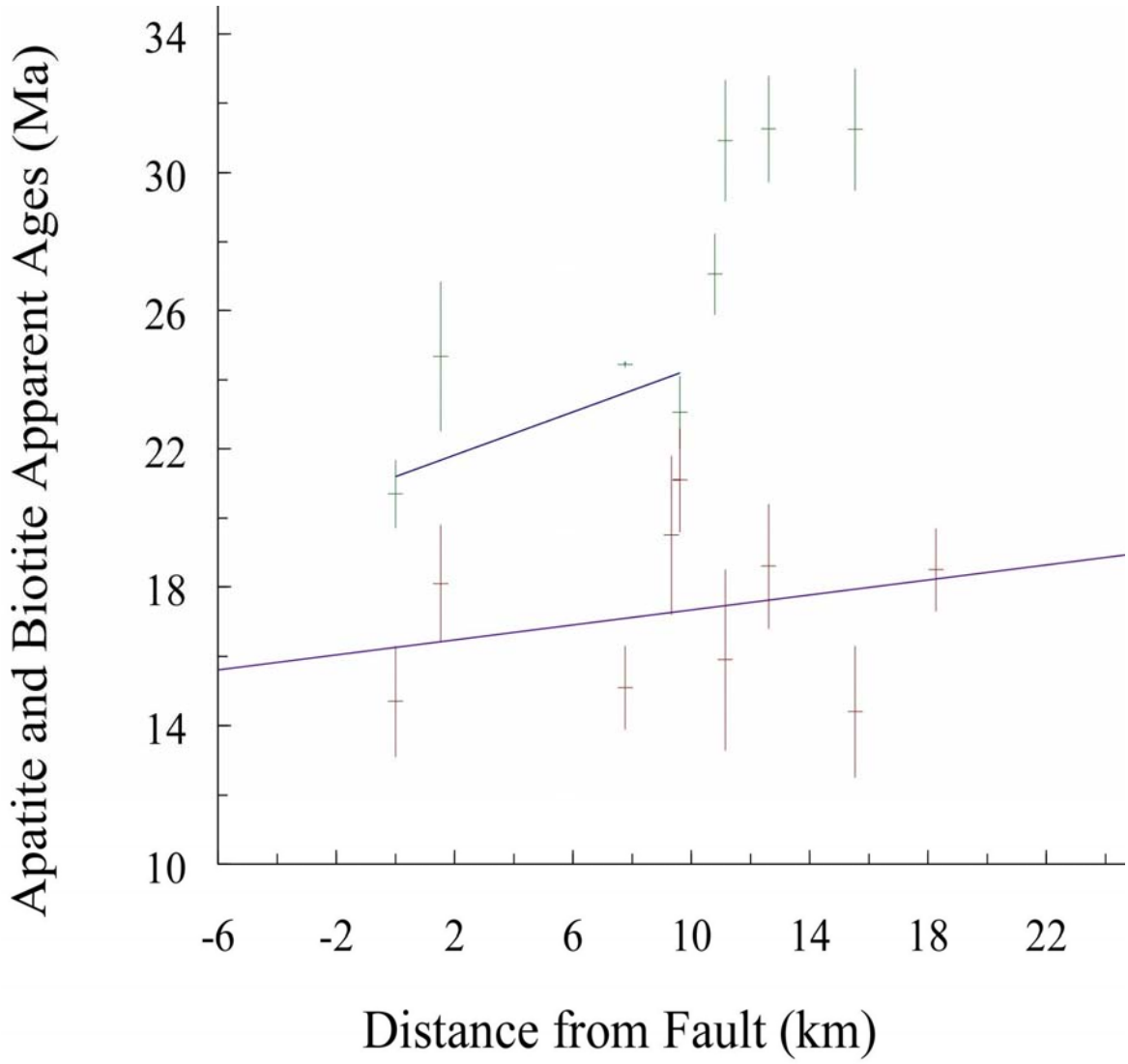

Figure 6-1. Apatite and biotite apparent ages vs. distance from fault. This graph was generated in ISOPLOT using the same methods as the individual data sets. Apatite data is graphed as red error crosses, biotite is graphed as green error crosses. The slope of the regression line on the younger four biotite apparent ages is 0.4 ± 1.7. The slope of the regression line on the apatite apparent ages is 0.11 ± 0.32. Error crosses are 2σ.

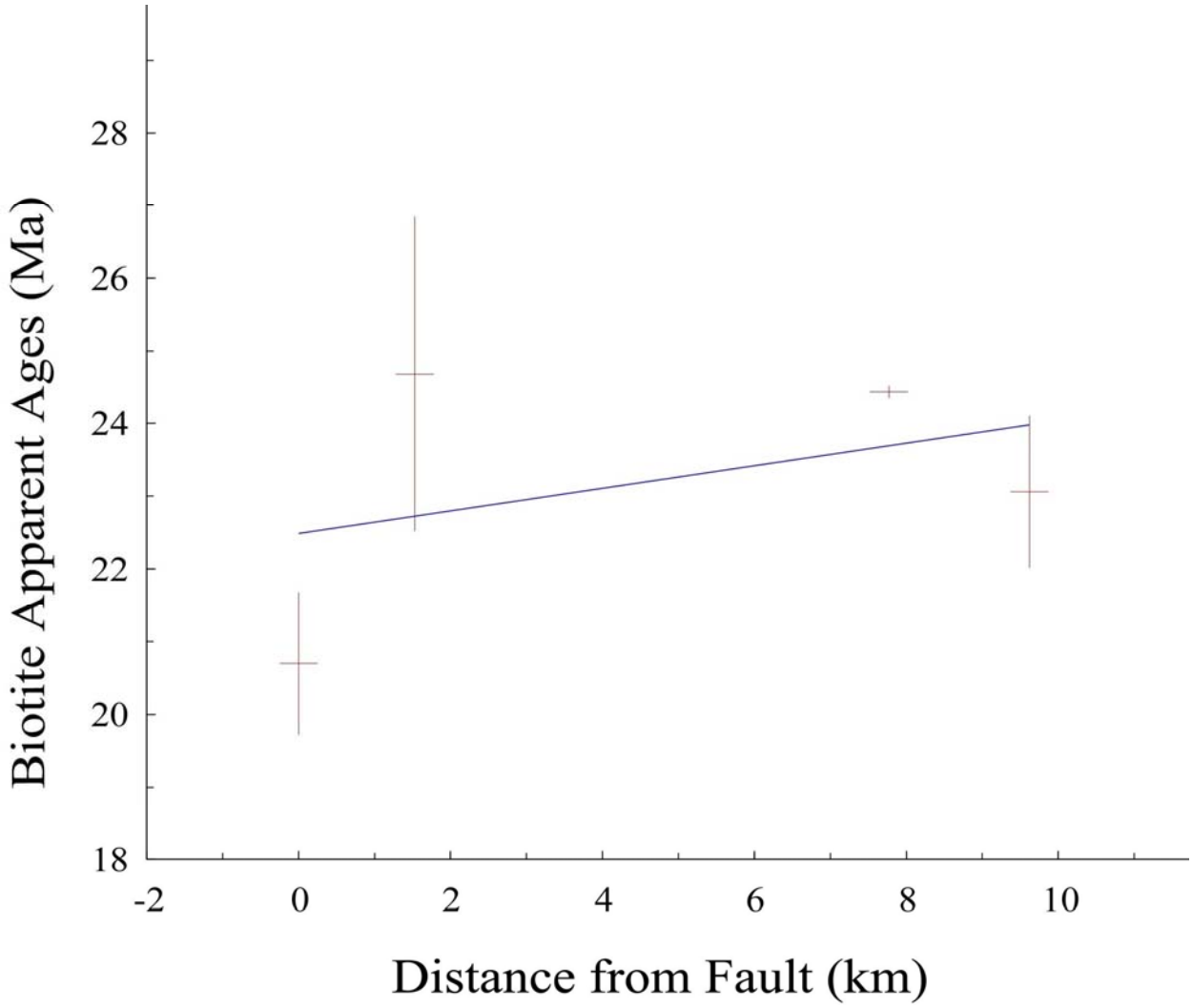

Figure 6-2. The younger biotite apparent ages vs. distance from fault. The graph was generated in ISOPLOT using the same methods as for the entire biotite data set. The slope of the regression line is 0.4 ± 1.7. The Mean Squared Weighted Deviates (MSWD) of the regression is 12. Error crosses are 2σ.

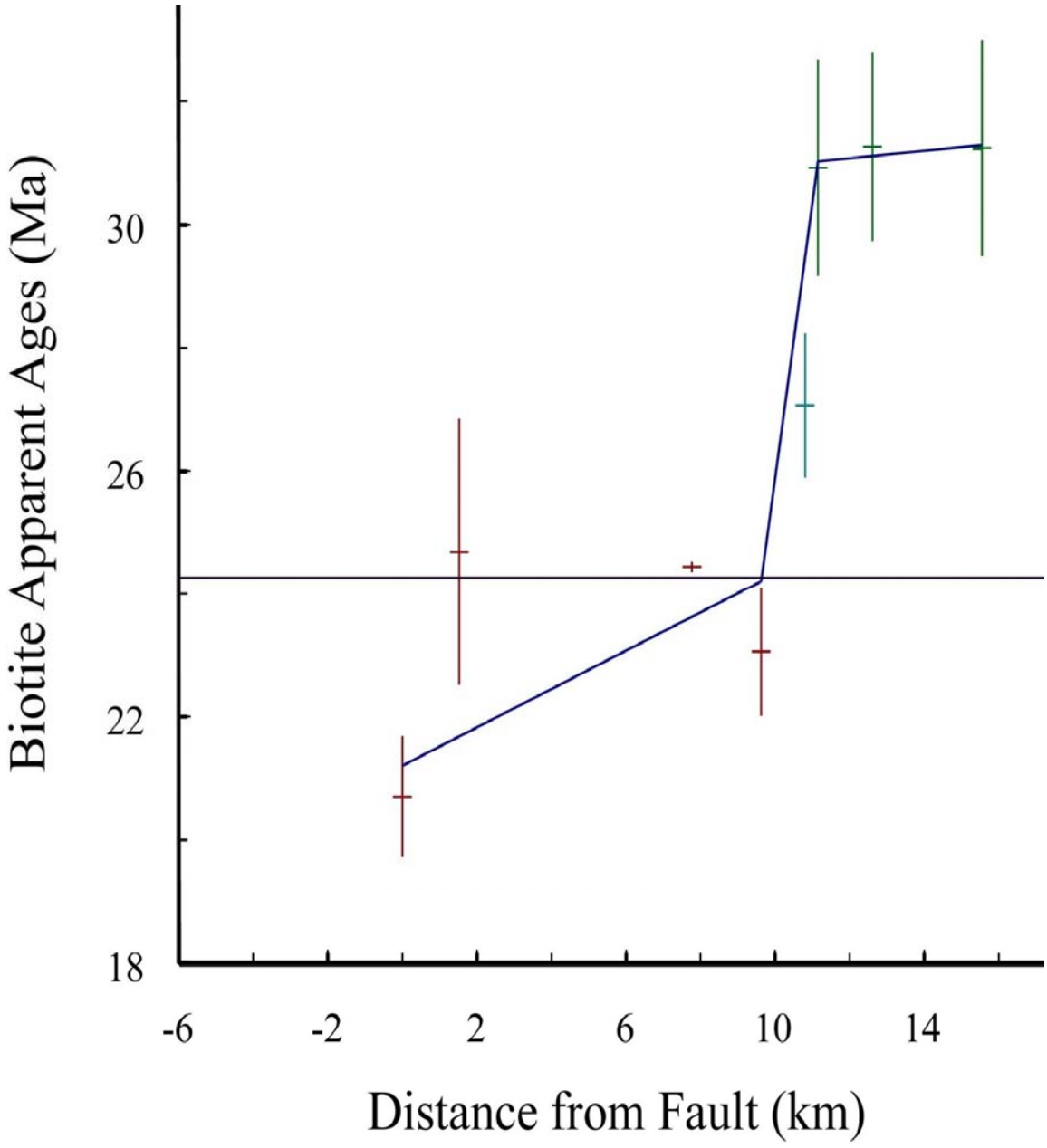

Figure 6-3. Base of the biotite argon partial retention zone at ca. 24 Ma. This graph was generated in ISOPLOT by the same method as the other graphs. The trend lines were also generated in ISOPLOT. The transition line between the two trend lines was drawn in Illustrator to clarify where the base of the biotite argon partial retention zone is located. The ca. 24 Ma line, black, was created to show the change in slope between the Illustrator line and the ISOPLOT trend line. Younger biotite apparent ages are represented by red error crosses, older biotite apparent ages are represented by green error crosses, and the teal error cross represents the biotite that plotted within the biotite argon partial retention zone. Error crosses are 2σ.

CHAPTER 7
CONCLUSIONS

The data obtained in this study are consistent with the hypotheses that rocks exposed in the Ruby Mountains metamorphic core complex were rapidly exhumed by a detachment fault. A possible second phase of brittle faulting and erosional exhumation at approximately 15 Ma is suggested by the apatite fission-track data. These thermochronologic data indicate that rapid exhumation took place during Miocene time, with an onset of approximately 24Ma. The apatite fission-track data suggest a rate of slip on the detachment of approximately 9.1 ± 3.1 km/my, which may record low angle faulting and subsequent brittle faulting. An apparently slower rate of 2.4 ± 0.6 km/my was calculated from the quenched biotite cooling ages.

APPENDIX A
METHODOLOGY

The samples utilized in this study were crushed at the U.S. Geological Survey. They were then washed to float the dust off and sieved in 60 to 120 mesh sieves. The 60 and 120 mesh fraction was used for thermochronology preparation. The samples were passed through pure tetrabromoethylene (TBE), specific gravity 2.96, to separate quartz, feldspars and other light minerals from heavier mafic minerals. The sinks were sent through the Frantz magnetometer to separate the magnetic minerals from the nonmagnetic. The magnetic fractions contained predominantly amphibole and mica. The nonmagnetic fractions primarily contained apatite and zircon. The nonmagnetic fractions were then passed through pure methyleneiodide (MI), specific gravity 3.32, to separate apatite from zircon. Following inspection under the binocular microscope the apatite separates were sent to Apatite to Zircon, Inc. for fission-track analysis. The magnetic fractions were inspected under a binocular microscope and picked when necessary for biotite, muscovite in one case, and amphibole. The original TBE floats were sent through a dilute solution of TBE in order to separate potassium feldspars from plagioclase. Additional field work was done in September, 2004.

Apatite fission-track data and $^{40}Ar/^{39}Ar$ thermochronology data were utilized to constrain the timing of the onset of slippage along the detachment fault as well as the time averaged rate of slippage along the fault.

APPENDIX B
APATITE FISSION-TRACK AGE AND LENGTH DATA

Apatite fission-track age and fission-track length data were obtained from Ray Donelick at Apatite to Zircon, Inc.

Table B-1. Apatite fission-track age data

ρs (10^6 tracks cm^-2)	N (tracks)	ρi (10^6 tracks cm^-2)	Ni (tracks)	ρd (10^6 tracks cm^-2)	Pooled Fission-Track Age (Ma)	Mean Fission-Track Age (Ma)	Median Fission-Track Age (Ma)
0.478	212	1.725	2060	3.795	20.4±1.6	21.1±1.5	20.4 0.7-1.6+
0.088	104	1.101	1298	3.818	16.0±1.7	19.5±2.3	17.3 1.2-3.4+
0.036	43	0.521	627	3.842	13.8±2.2	15.9±2.6	13.8 2.0-2.7+
0.508	607	5.698	6803	3.889	18.1±0.9	18.5±1.2	18.5 0.7-0.7+
0.084	98	1.081	1254	3.913	16.0±1.7	14.4±1.9	15.7 2.3-1.1+
0.082	98	0.086	1173	3.936	17.2±1.9	18.6±1.8	17.1 1.4-1.0+
0.501	588	7.155	8390	3.96	14.5±0.7	15.1±1.2	14.1 1.1-1.3+
0.172	198	2.034	2340	3.984	17.6±1.4	18.1±1.7	16.0 1.4-1.8+
0.063	71	0.935	1056	4.007	14.1±1.8	14.7±1.6	14.4 2.0-1.7+

ρ_s is the density of spontaneous fission-tracks, N is the number of fission-tracks, ρ_i is the density of induced fission-tracks, N_i is the number of induced fission-tracks, and ρ_d is the density of induced fission-tracks in the dosemeter.

Table B-2. Apatite fission-track length data.

Sample Numbers	Tracks	Mean± Standard Error (μm)	Standard Deviation (μm)	5-6	6-7	7-8	8-9	9-10	10-11	11-12	12-13	13-14	14-15	15-16	16-17	17-18
H93Ruby-4	131	14.73 0.11	1.25	0	0	0	0	0	2	1	9	16	49	34	16	4
H93Ruby-5	63	14.60 0.13	1.05	0	0	0	0	0	0	1	4	10	23	20	5	0
H93Ruby-8	82	14.54 0.10	0.9	0	0	0	0	0	0	1	4	15	36	22	4	0
H97Ruby-41	129	14.57 0.11	1.19	0	0	0	1	0	0	0	12	24	41	39	11	1
H97Ruby-42	25	14.86 0.22	1.07	0	0	0	0	0	0	0	1	4	9	8	2	1
H97Ruby-51	97	14.65 0.10	1	0	0	0	0	0	0	2	4	13	46	23	7	2
H97Ruby-53	142	14.58 0.09	1.02	0	0	0	0	0	0	0	10	35	47	41	7	2
H97Ruby-54	137	14.06 0.13	1.55	0	0	0	0	1	4	3	17	28	48	28	5	2
H97Ruby-55	89	14.21 0.14	1.33	1	0	0	0	1	3	2	4	24	31	21	2	1

APPENDIX C
MONTE TRAX APATITE FISSION-TRACK MODELS

Figures 1 through 9 are individual runs showing best-fit lines generated by the Monte Trax program (Gallagher, 1995). In order to generate these figures, broad time and temperature boundaries were input, as well as the observed mean fission-track ages. A genetic algorithm was then used to select time-temperature points from within the initial time-temperature boundaries and construct a thermal history. Built-in statistical tests determine which is the best-fit model for each sample. The track length histograms were created by inputting individual grain counts and track length measurements into the program. Data used to create these models is listed in Appendix B.

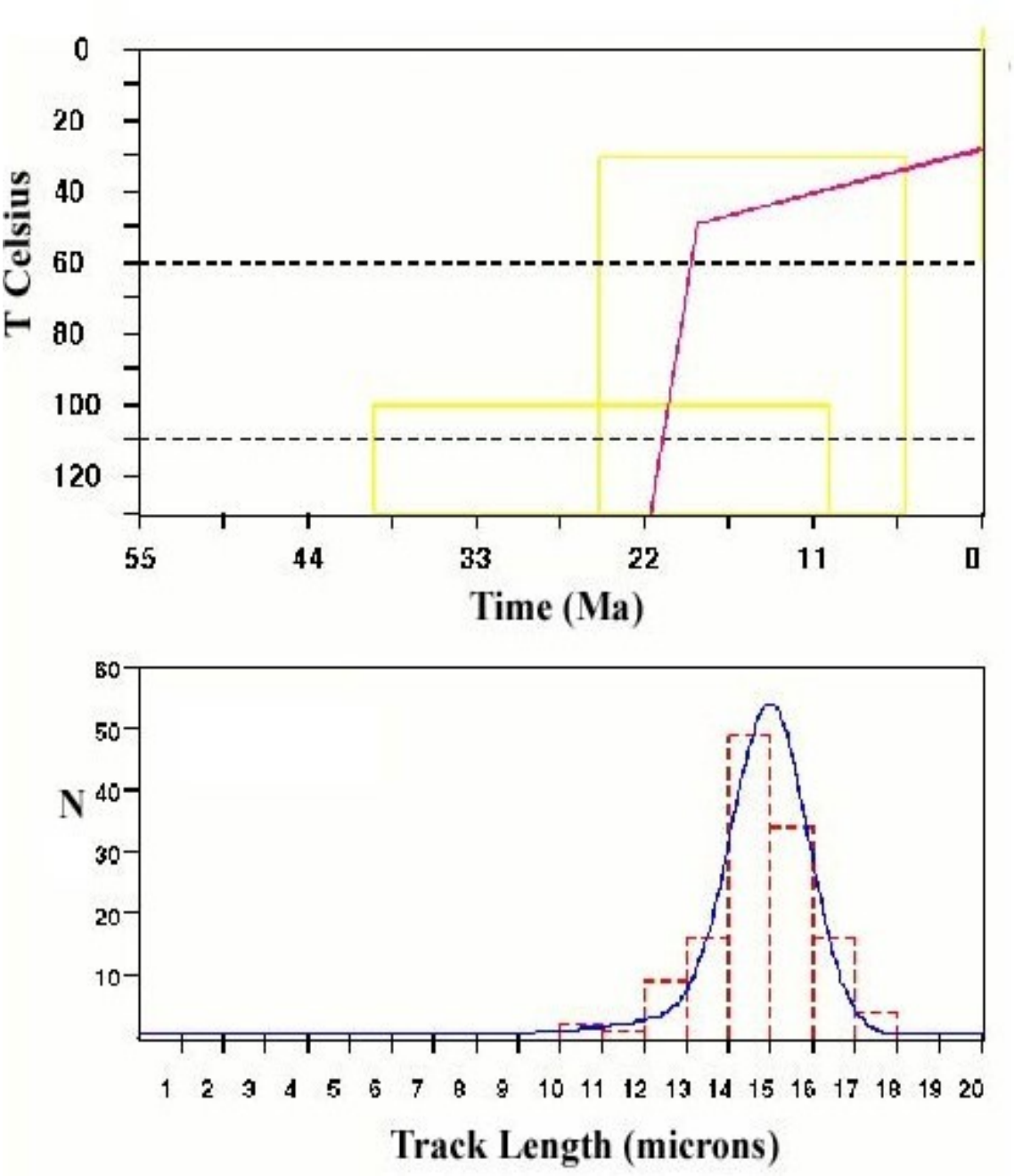

Figure C-1. Best fit Monte Trax model for H93 RUBY-4. Observed age is 21.10 Ma, predicted age is 21.05 Ma. Observed mean track length is 14.730 µm, predicted mean track length is 14.735 µm. Observed standard deviation is 1.250, predicted standard deviation is 1.271. This model run indicates rocks were at 150°C at 23 Ma, 49°C at 19 Ma, and 29°C at 0 Ma.

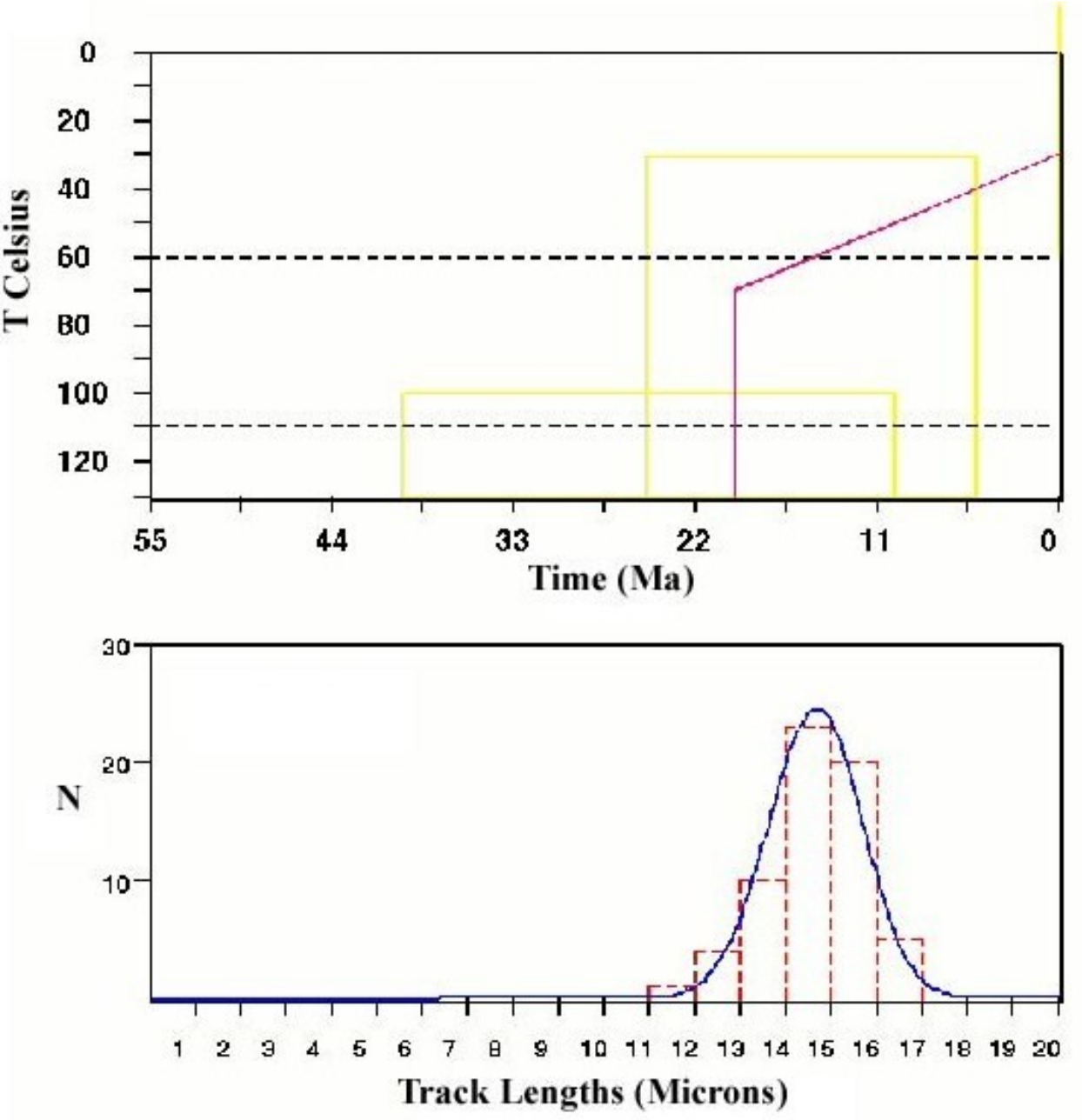

Figure C-2. Best fit Monte Trax model for H93RUBY-5. Observed age is 19.50 Ma, predicted age is 19.10 Ma. Observed mean track length is 14.600 µm, predicted mean track length is 14.603 µm. Observed standard deviation is 1.050, predicted standard deviation is 1.056. This model run indicates that rocks were at 196°C at 20 Ma, 69°C at 20 Ma, and 30°C at 0 Ma.

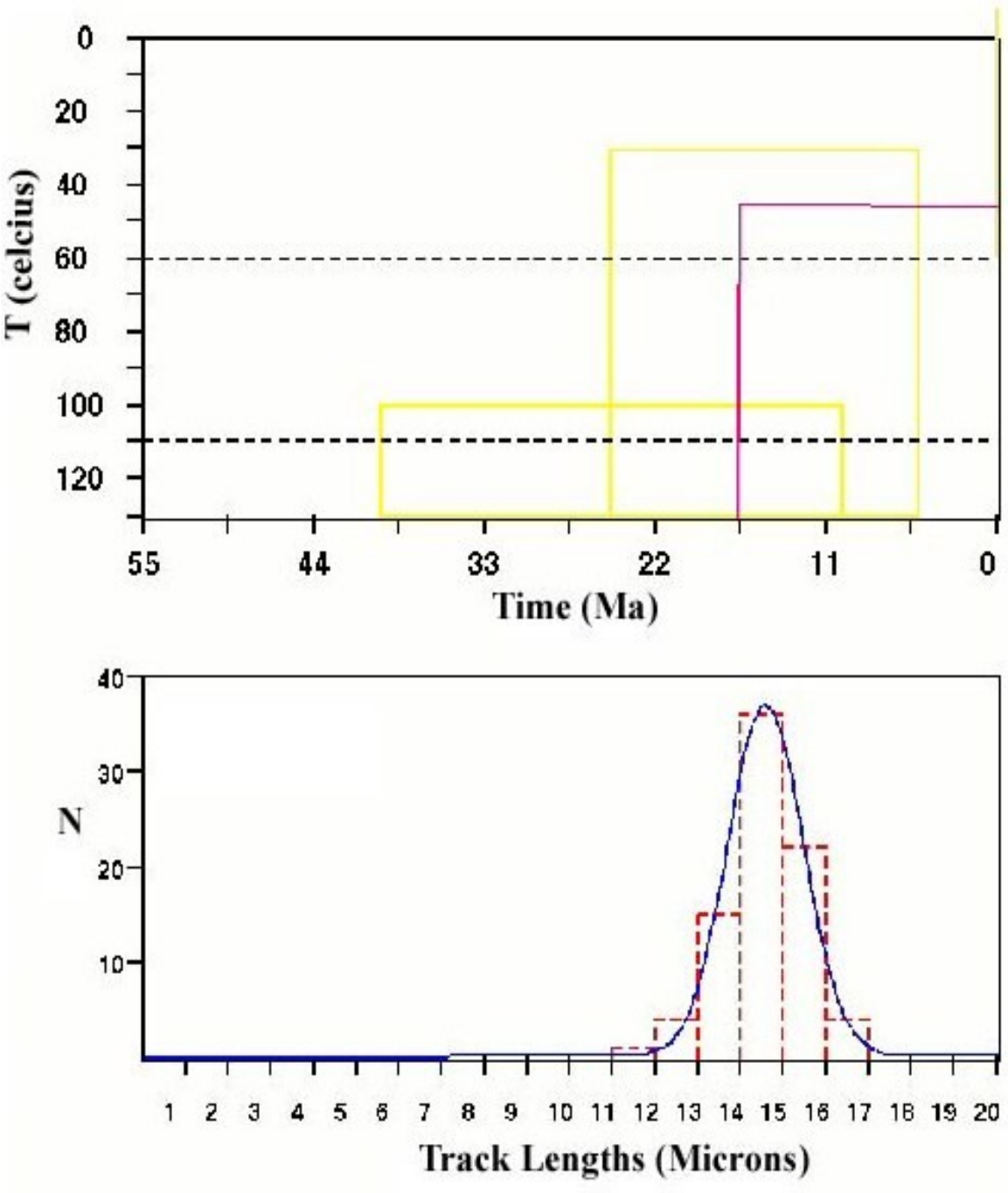

Figure C-3. Best fit Monte Trax model for H93RUBY-8. Observed age is 15.90 Ma, predicted age is 16.13 Ma. Observed mean track length is 14.540 µm, predicted mean track length is 14.565 µm. observed standard deviation is 0.900, predicted standard deviation is 0.935. This model run indicates rocks were at 163°C at 17 Ma, 46°C at 17 Ma, and 47°C at 0 Ma.

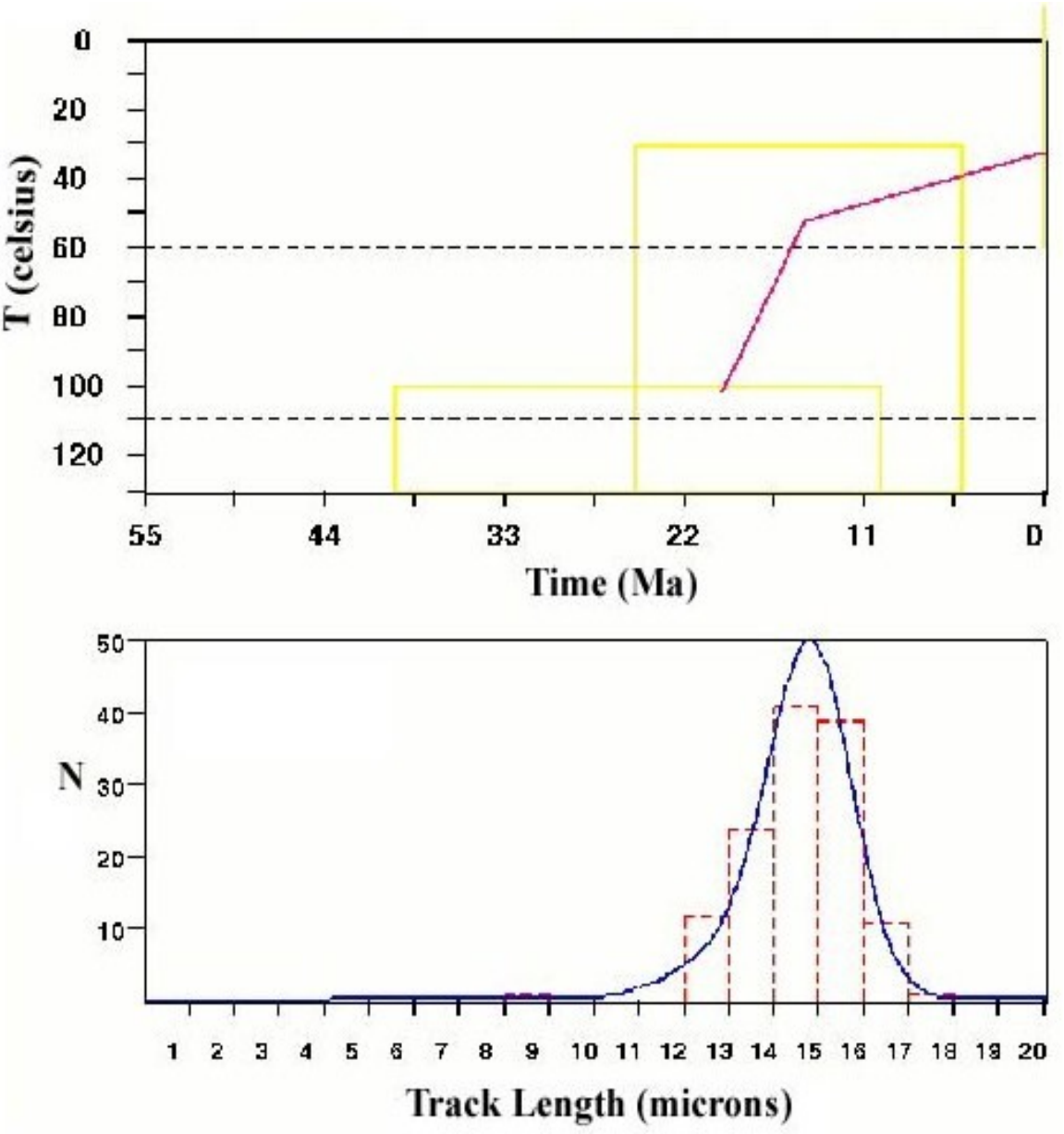

Figure C-4. Best fit Monte Trax model for H97RUBY-41. Observed age is 18.50 Ma, predicted age is 19.01 Ma. Observed mean track length is 14.570 µm, predicted mean track length is 14.534 µm. Observed standard deviation is 1.190, predicted standard deviation is 1.186. This model run indicates rocks were at 102°C at 20 Ma, 52°C at 15 Ma, and 33°C at 0 Ma.

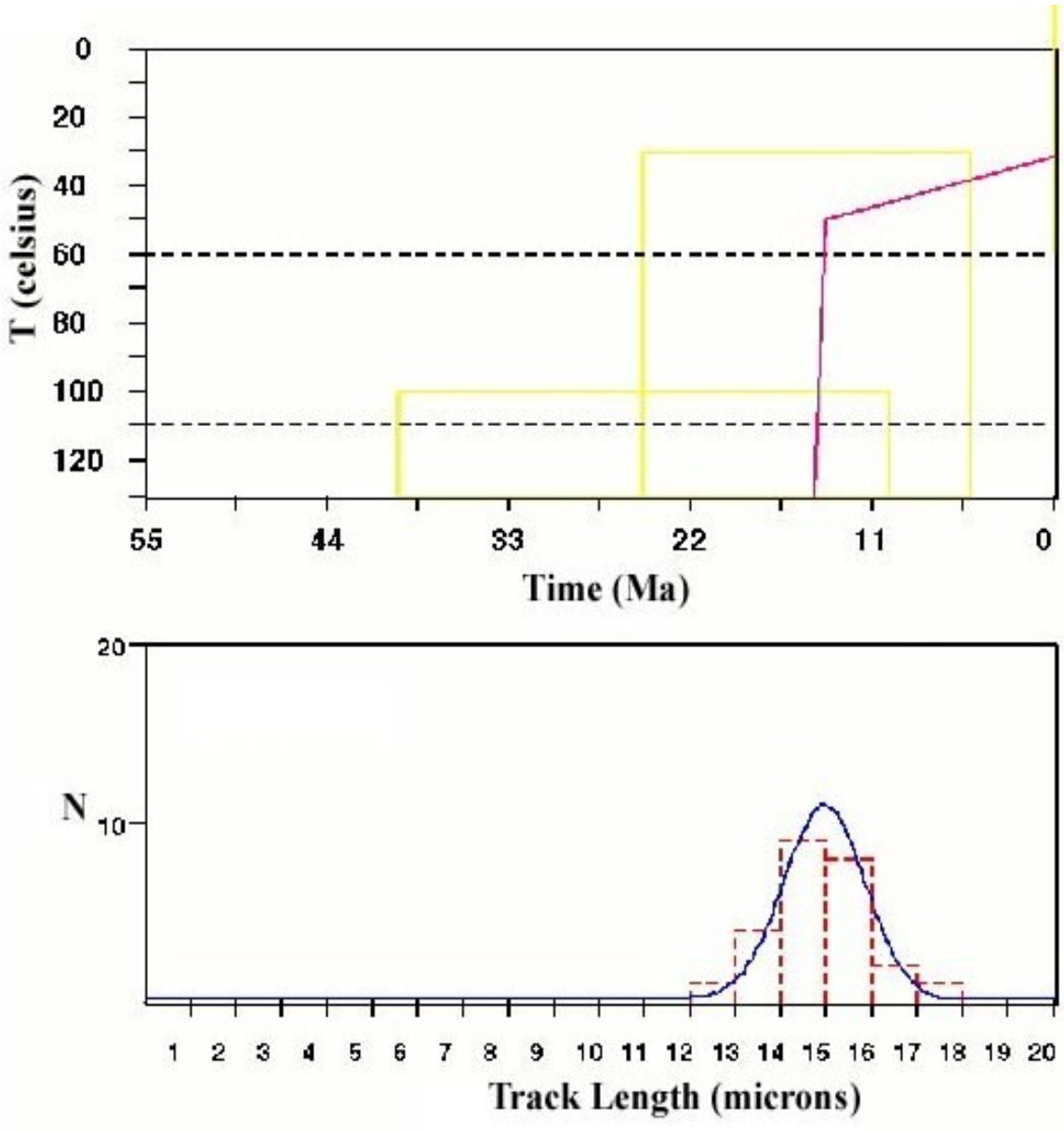

Figure C-5. Best fit Monte Trax model for H97RUBY-42. Observed age is 14.40 Ma, predicted age is 14.35 Ma. Observed mean track length is 14.860 µm, predicted mean track length is 14.862. Observed standard deviation is 1.070, predicted standard deviation is 1.067. This model run indicates that rocks were at 152°C at 15 Ma, 50°C at 14 Ma, and 32°C at 0 Ma.

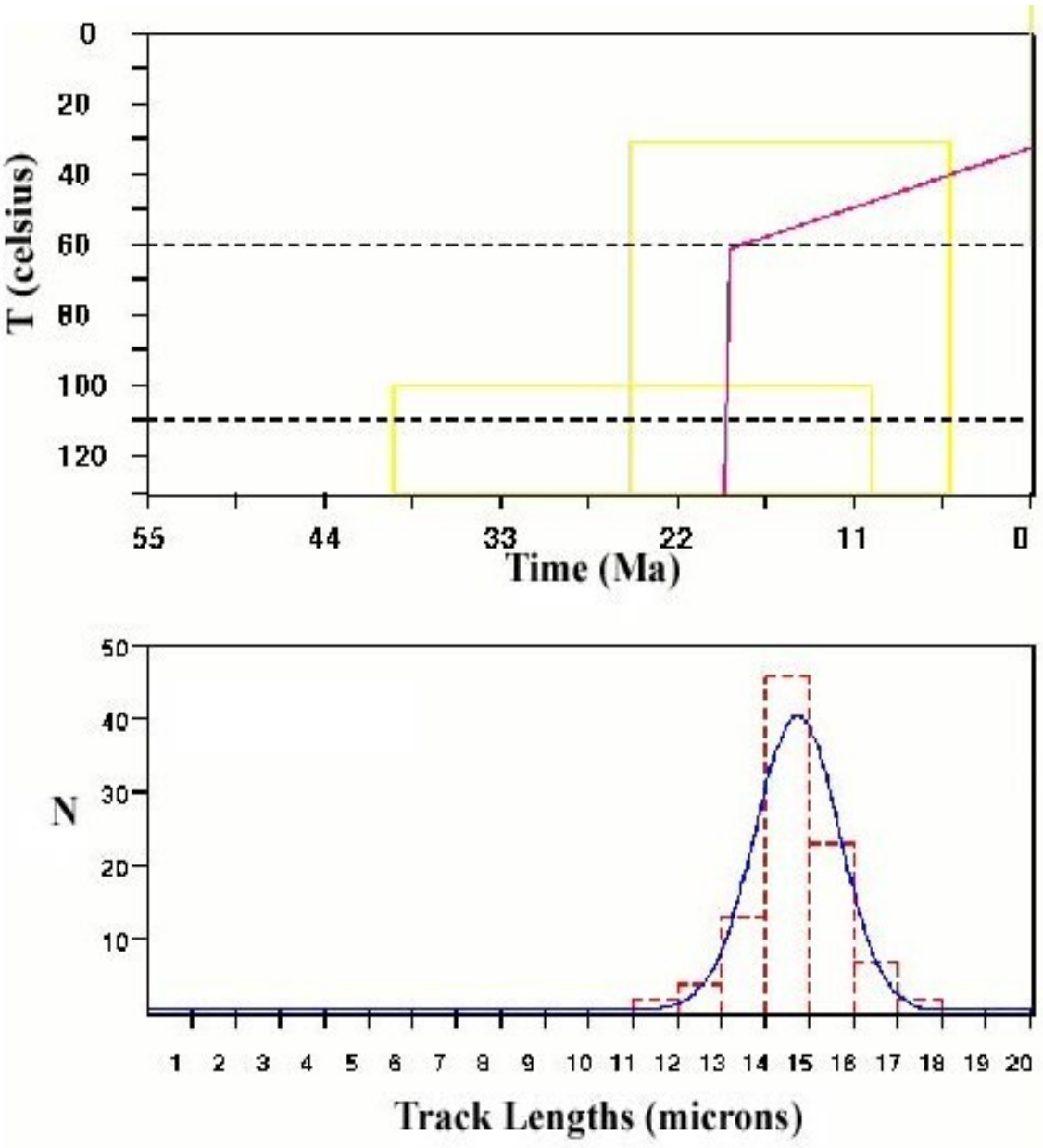

Figure C-6. Best fit Monte Trax model for H97RUBY-51. Observed age is 18.60 Ma , predicted age is 18.61 Ma. Observed mean track length is 14.650 µm, predicted mean track length is 14.662 µm. Observed standard deviation is 1.000, predicted standard deviation is 1.027. This model run indicates that rocks were 143°C at 19 Ma, 61°C at 19 Ma, and 33°C at 0 Ma.

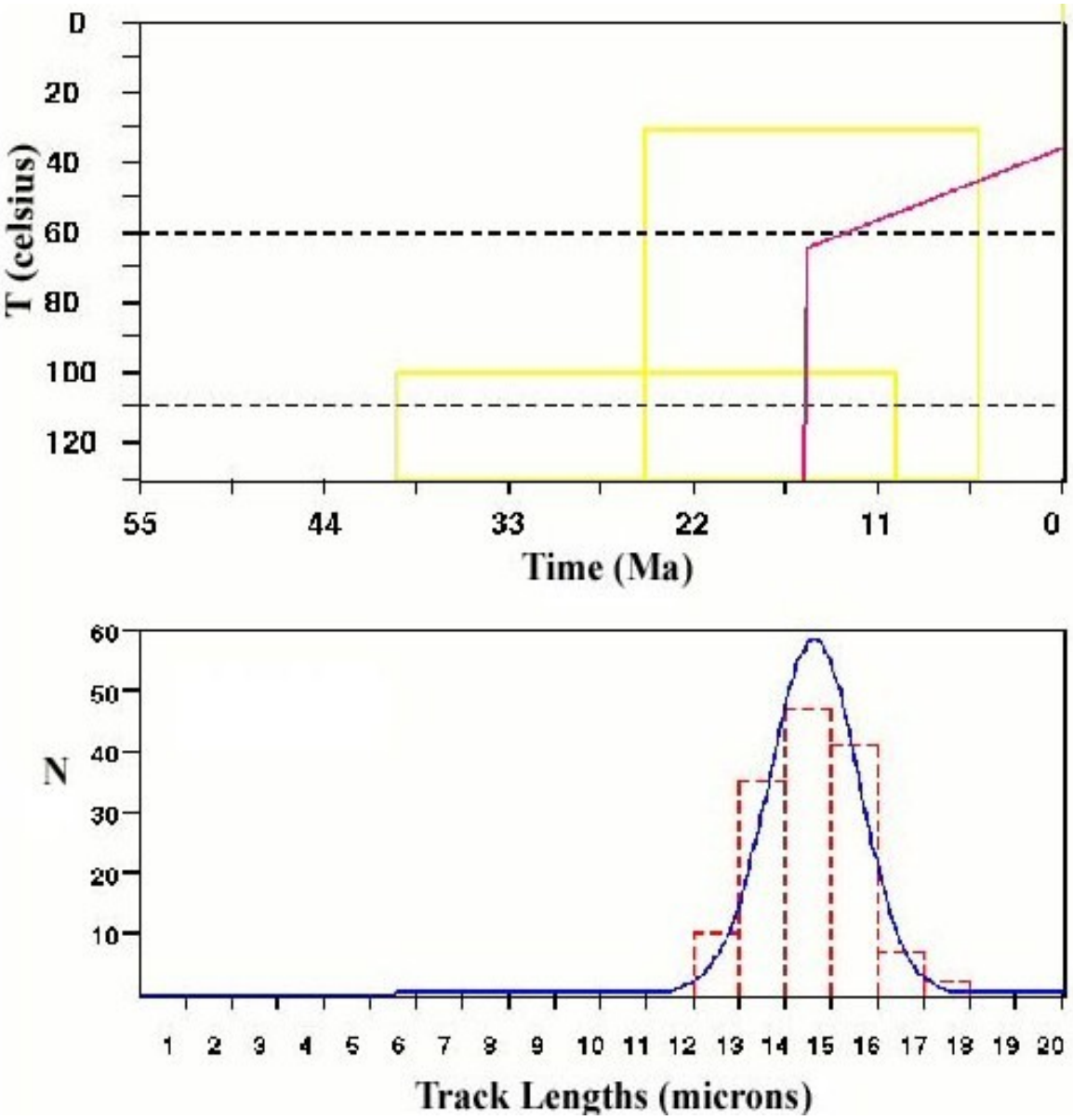

Figure C-7. Best fit Monte Trax model for H97RUBY-53. Observed age is 15.10 Ma, predicted age is 15.04 Ma. Observed mean track length is 14.580 µm, predicted mena track length is 14.569 µm. Observed standard deviation is 1.020, predicted standard deviation is 1.016. This model run indicates that rocks were at 195°C at 16 Ma, 65°C at 15 Ma, and 36°C at 0 Ma.

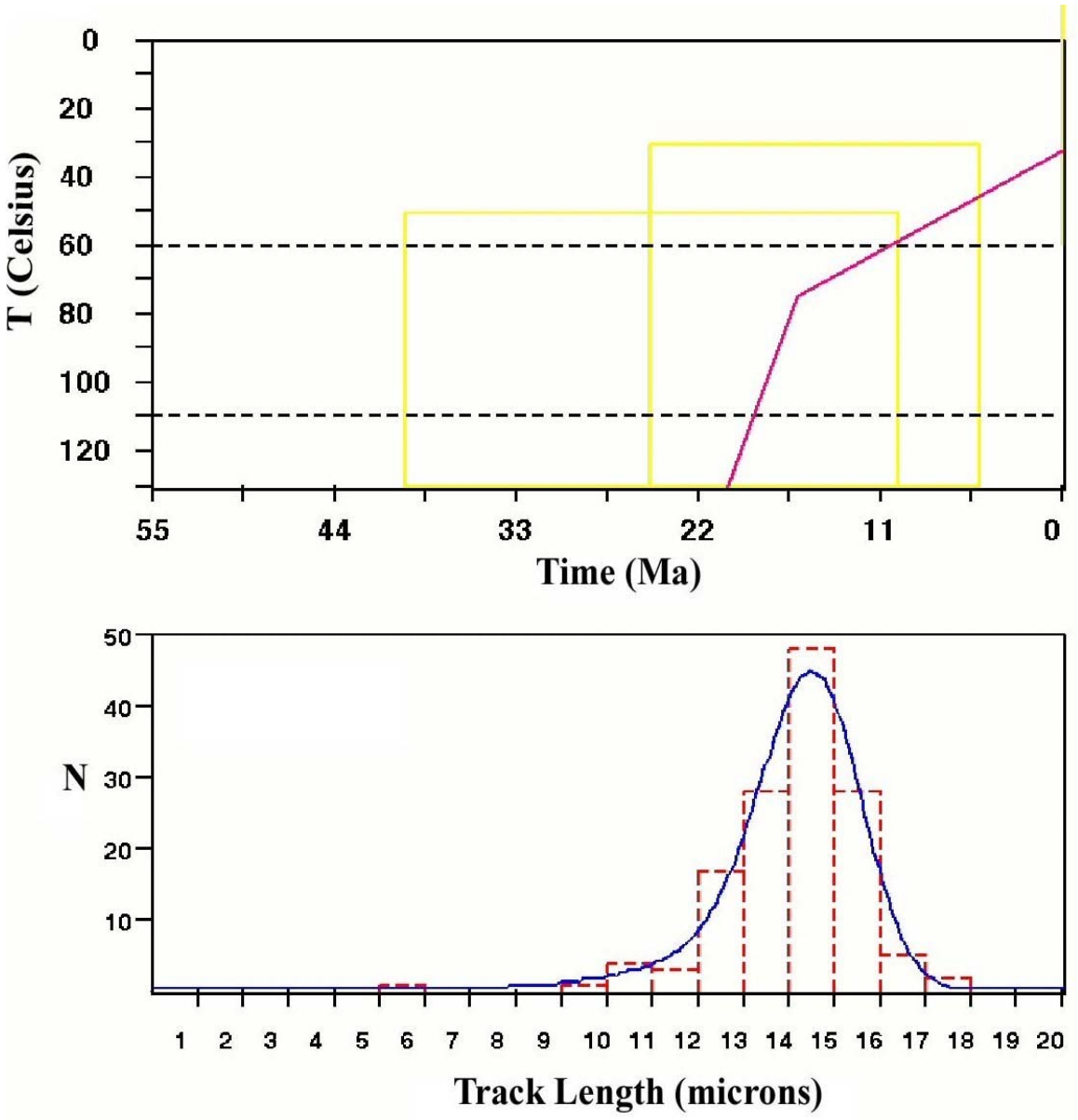

Figure C-8. Best fit Monte Trax model for H97RUBY-54. Observed age is 18.10 Ma, predicted age is 18.10 Ma. Observed mean track length is 14.060 µm, predicted mean track length is 14.072 µm. Observed standard deviation is 1.550, predicted standard deviation is 1.517. This model run indicates that rocks were 237°C at 28 Ma, 75°C at 16 Ma, and 33°C at 0 Ma.

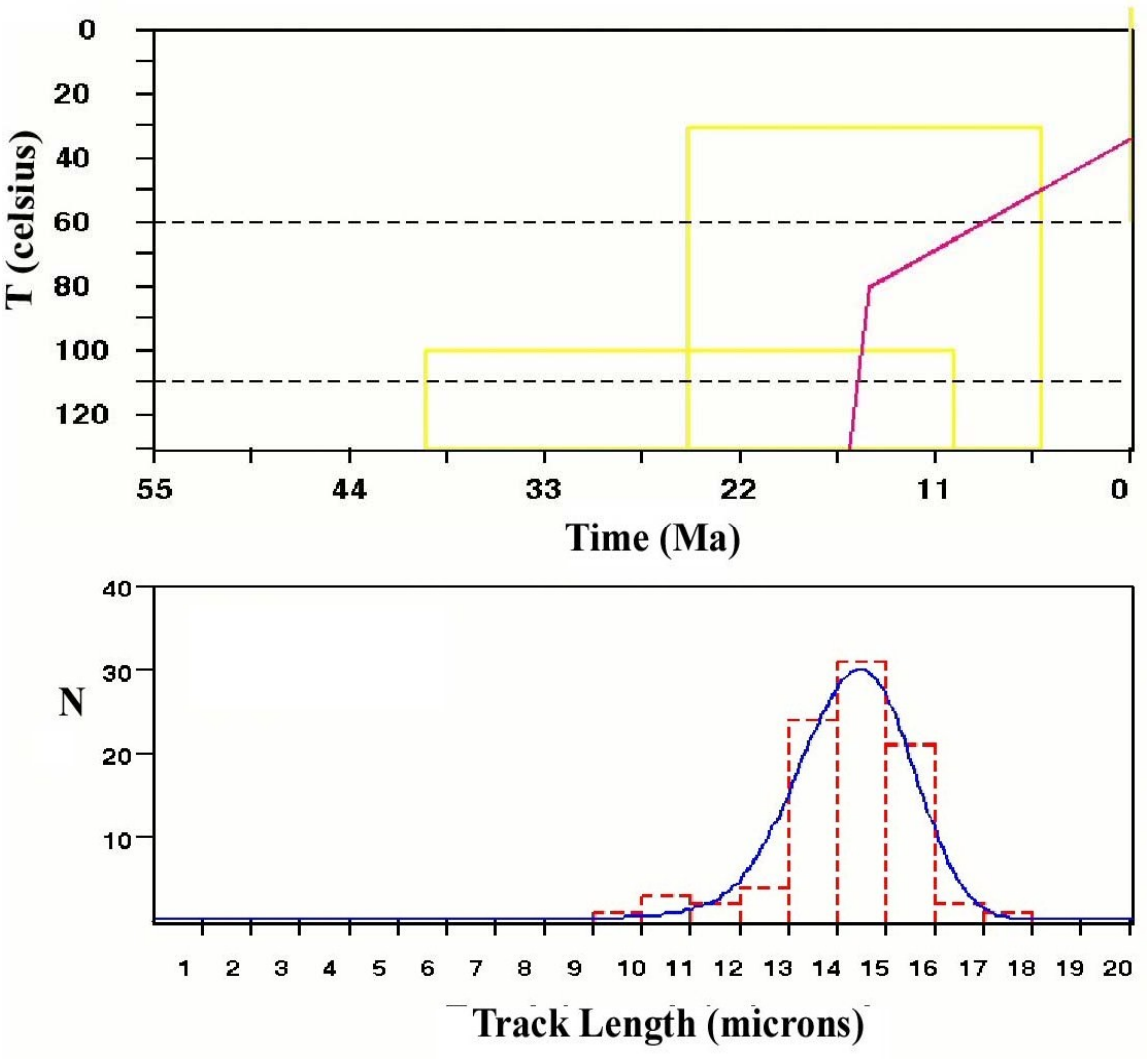

Figure C-9. Best fit Monte Trax model for H97RUBY-55. Observed age is 14.70 Ma, predicted age is 14.80 Ma. Observed mean track length is 14.210 µm, predicted mean track length is 14.198 µm. Observed standard deviation is 1.330, predicted standard deviation is 1.320. This model run indicates that rocks were 174°C at 17 Ma, 80°C at 15 Ma, and 34°C at 0 Ma.

LIST OF REFERENCES

Armstrong, R. L., and Ward, P., 1991, Evolving geographic patterns of Cenozoic magmatism in the North American cordillera: The temporal and spatial association of magmatism and metamorphic core complexes: Journal of Geophysical Research, v. 96, p. 13,201-13,224.

Best, M. G., and Christiansen, E. H., 1991, Limited extension during peak Tertiary volcanism, Great Basin of Nevada and Utah: Journal of Geophysical Research, v. 96, p. 13,509-12,528.

Buck, W., 1988, Flexural rotation of normal faults: Tectonics, vol.7, i. 5, p. 959-973.

Burchfiel, B. C., Cowan, D. S., Davis, G. A., 1992, Tectonic overview of the cordilleran orogen in the western United States: The geology of North America: The Geological Society of America, v. G-3, p. 407-479.

Camilleri, P. A., and Chamberlain, K. R., 1997, Mesozoic tectonics and metamorphism in the Pequop Mountains and Wood Hills region, northeast Nevada: Implications for the architecture and evolution of the Sevier orogen: Geological Society of America Bulletin, v. 109, i. 1, p. 74-94.

Carter, T. J., Kohn, B. P., Foster, D. A., and Gleadow, A. J. W., 2004,How the Harcuvar Mountains metamorphic core complex became cool: Evidence from apatite (U-Th)/He thermochronometry: Geology, v. 32, n. 11, p. 985-988.

Carter, T. J., Kohn, B. P., Foster, D. A., Gleadow, A. J. W., and Woodhead, J. D., 2006, Late-stage evolution of the Chemehuevi and Sacramento detachment faults from apatite (U-Th)/He thermochronometry: Evidence for mid-Miocene accelerated slip: Geological Society of America Bulletin, v.118, n. 5/6, p. 698-709.

Colgan, P. A., Metcalf, J. R., 2006, Rapid middle Miocene unroofing of the southern Ruby Mountains, Nevada: Geological Society of America Abstracts with Programs, v. 38, n. 7, p. 417.

Colgan, P. A., Dumitru, T. A., McWilliams, M, and Miller, E. L., 2006, Timing of Cenozoic volcanism and Basin and Range extension in northeastern, Nevada: New constrainsts from the northern Pine Forest Range: Geological Society of America Bulletin, v. 118, i. 1, p. 126-139.

Coney, P. J., and Harms, T. A., 1984, Cordilleran metamorphic core complexes: Cenozoic extensional relics of Mesozoic compression: Geology, v. 12, p.550-554.

Crittendon, M., Jr., Coney, P. J., and Davis, G., 1977, Tectonic significance of metamorphic core complexes in the North American cordillera: Geology, v.6, p. 79-80

Dallmeyer, R. D., Snoke, a. W., and McKee, E. H., 1986, The Mesozoic-Cenozoic tectonothermal evolution of the Ruby Mountains-East Humboldt Range, Nevada: a cordilleran metamorphic core complex: Tectonic, v. 5, p. 931-954.

Dokka, R. K., and Mahaffie, M. J., 1986, Thermochronologic evidence of major tectonic denudation associated with detachment faulting, northern Ruby Mountians-East Humboldt Range, Nevada: Tectonics, v.5 p. 995-1006.

Donelick, R. A., O'Sullivan, B. P., and Ketcham, R. A., 2005, Apatite fission-track analysis: Reviews in Mineralogy and Geochemistry, v. 51; 1, p. 49-94.

Faure, G., 1986, Principles of Isotope Geology: New York, New York, John Wiley and Sons, Inc.

Foster, D. A., Gleadow, A. J. W., Reynolds, S. J., and Fitzgerald, P. G., 1993, Denudation of metamorphic core complexes and the reconstruction og the transition zone, west central Arizona: Constraints from apatite fission-track thermochronology: Journal of Geophysical Research, v. 98, p. 2167-2185.

Foster, D. A., and John, B. E., 1993, Structural and thermal constraints on the initiation angle of detachment faulting in the southern Basin and Range: The Chemehuevi Mountains case study: Geological Society of America, v. 105, p. 1091-1108.

Foster, D. A., and John, B. E., 1999, Quantifying tectonic exhumation in an extensional orogen witt thermochronology: Examples from the southern Basin and Range Province: Geological Society, London, Special Publications, v. 154, p. 343-364.

Gallagher, K., 1995, Monte Trax: On Track: The Newsletter of the International Fission-Track community, v. 5, n. 1, i. 10

Gallagher, K., Brown, R., and Johnson, C., 1998, Fission-track analysis and its application to geological problems: Annual Review of Earth and Planetary Sciences, v. 26, p. 519-572.

Gans, P., 1987, An open-system, two-layer crustal stretching model for the eastern Great Basin: Tectonics, v. 6, i. 1, p. 1-12.

Gifford, J., 2008, Quantifying Eocene and Miocene extension in the Sevier hinterland of the Ruby-East Humboldt metamorphic core complex in northeastern Nevada. Gainesville, Florida, The University of Florida, M. S. thesis, 90??p.

Gleadow, A. J. W., and Duddy, I. R., 1981, A natural long-term annealing experiment for apatite: Nuclear Tracks and Radiation Measurements, v. 5, p. 169-174.

Gleadow, A. J. W., and Brown, R. W., 1999, Fission-track thermochronology and the long-term denudational response to tectonics, In (Ed.), Summerfield, M. A., Geomorphology and Global Tectonics, John Wiley and Sons LTD., Chichester, p. 57-75.

Hacker, B. R.,Yin, A., and Christie, J. M., 1990, Differential stress, strain rate, and temperatures of mylonization in the Ruby Mountains, Nevada: Journal of Geophysical Researcg, v. 95, p. 8569-8580.

Hodges, K. V., Snoke, A. W., and Hurlow, H. A., 1992, Thermal evolution of a portion of the Sevier hinterland: The Ruby Mountain-East Humboldt Range and Wood Hills, northeastern Nevada: Tectonics, v. 11, p. 154-164.

Howard, K. A., 1971, Paleozoic metasediments in the northern Ruby Mountains, Nevada: Geological Society of America Bulletin, v. 82, p. 259-264.

Howard, K. A., 1980, Metamorphic infrastructure in the northern Ruby Mountains, Nevada: Geological Society of America, Memoir 153, p. 335-347.

Hurlow, H. A., Snoke, A. W., and Hodges, K. V., 1991, Temperature and pressure mylonization in a Tertiary extensional shear zone, Ruby Mountain-East Humboldt Range, Nevada: Tectonic implications: Geology, v. 19, p. 82-86.

Kistler, R. W., Ghent, E. D., and O'Neil, J. R., 1981, Petrogenesis of garnet two-mica granites in the Ruby Mountains, Nevada: Journal of Geophysical Research, v. 86, p. 10,597-10,606.

Koppers, A. A. P., 2002, ArArCALC, software for $^{40}Ar/^{39}Ar$ age calculations: Computers and Geosciences, v. 5, p. 605-619.

Lee, J., and Sutter, J. F., 1991, Incremental $^{40}Ar/^{39}Ar$ thermochronology of mylonitic rocks from the northern Snake Range, Nevada: Tectonic, v. 10, p. 77-100.

Ludwig, K. R., 2004, User's manual for ISOPLOT, a geochemical toolkit for Microsoft Excel (v. 3.09a).

MacCready, T., Snoke, A. W., Wright, J. E., and Howard, K. A., 1997, Mid-crustal flow during Tertiary extension in the Ruby Mountains core complex, Nevad: Geological Society of America Bulletin, v. 109, p. 1576+1594.

McDougall, I., and Harrison, T. M., 1999, Geochronology and Thermochronology by the $^{40}Ar/^{39}Ar$ Method: New York, New York, Oxford University Press, Oxford, UK.

McGrew, A. J., and Snee, L. W., 1994, Ar/Ar thermochronologic constraints on the tectonothermal evolution of the northern East Humboldt Range metamorphic core complex, Nevada: Tectonophysics, v. 238, p. 425-450.

McGrew, A. J., Peters, M. T., and Wright, J. E., 2000, Thermobarometric constraints on the tectonothermal evolution of the East Humboldt Range metamorphic core complex, Nevada: Geological Society of America Bulletin, v. 112, p. 45-60.

Mueller, K. J., Cerveny, P. K., Perkins, M. E., and Snee, L. W., 1999, Chronology of polyphase extension in the Windermere Hills, northeast Nevada: Geological Society of America Bulletin, v. 111, p. 11-27.

Mueller, K. J., and Snoke, A. W., 1993, Progressive overprinting of normal fault systems and their role in Tertiary exhumation of the East Humboldt-Wood Hills metamorphic complex northeast Nevada: Tectonics, v. 12, p. 361-371.

Reese, N. M., 1983, Cenozoic tectonic history of the Ruby Mountains and adjacent areas, northeastern Nevada: Constraints from radiometric dating and seismic reflection profiles: Dallas, Texas, Southern Methodist University, M. S. thesis, 88p.

Sharp, R. P., 1938, Structure of the Ruby-East Humboldt Range: Geological Society of America Bulletin, v. 50, p. 881-917.

Snoke, A. W., Howard, K. A., McGrew, A. J., Burton, B. R., Barnes, C. G., Peters, M. T., and Wright, J. E., 1997, The grand tour of the Ruby-East Humboldt metamorphic core complex, northeaster Nevada: Part I-Introduction and road log: BYU Geology Studies, v. 42, part 1, p. 225-269.

Sonder, L. J., and Jones, C. H., 1999, Western United States extension: How the west was widened: Annual Review of Earth and Planetary Sciences, v. 27, p. 417-462.

Stockli, D. F., Linn, J. K., Dumitru, T. A., and Miller, E. L., 2001, Miocene unroofing of the Canyon Range durin extension along the Sevier Desert Detachment, west central Utah: Tectonics, v. 20, p. 289-307.

Stockli, D. F., 2005, Application of low-temperature thermochronometry of extensional tectonic settings: Reviews in Mineralogy and Geochemistry, v. 58, p. 411-448.

Wells, M., Snee, L., and Blythe, A., 2000, Dating of major normal fault systems using thermochronology: an example from the Raft River detachment: Basin and Range, western United Staes: Journal of Geophysical Research, v. 105(B7), p. 16303-16327.

Wernicke, B., 1992, Cenozoic extensional tectonics of the U.S. cordillera: The Geology of North America: The Geological Society of America, v. G-3, p. 553-579.

Wernicke, B., and Axen, G. J., 1988, On the role of isostacy in the evolution of normal fault systems: Geology, v. 16, p. 848-851.

BIOGRAPHICAL SKETCH

Virginia Newman was born in Melbourne, FL in 1975. She graduated from Deltona High School (with honors) in 1993. She earned a Bachelor of Arts degree in linguistics from the University of Florida–Gainesville in 1997. Virginia took several years off from education in order to marry and start a family. Once admitted to graduate school at the University of Florida, she spent a year as a teaching assistant. Virginia received a Master of Science degree from the University of Florida in May of 2008. Virginia will continue to pursue her interests in the geological sciences in the private sector.